POLITECNICO DI TORINO

Master's Degree in Ingegneria Biomedica

Master's Degree Thesis

Advanced deconvolution method for the estimation of motor nerve conduction block: test on patients and comparison with standard clinical methods

Supervisor	Candidate
Prof. Luca MESIN	Edoardo LINGUA

March 2021

Acknowledgements

First of all, i would like to express my special thanks of gratitude to Prof. Luca Mesin, who gave me the golden oppurtunity to do this extremely interesting thesis work related to the neuromuscolar system. His help and advices were constant throughout the whole period in which i worked on this project, allowing me to learn as much as possible from his experience and knowledge.
I would also like to extend my gratitude to Prof. Taian Vieira for providing me help and important material for my research and to Dr. Dario Cocito which provided the experimental signals and the medical knowledge.

My deepest gratitude goes to the most important people of my life, whose support was fundamental during all my universitary journey: my friends, my family and Giulia; thanks for the love and care you always demonstrated me.

Finally, i wish to dedicate this thesis to my beloved grandparents, whose teachings and love i will always carry in my heart and made me the man that i am today.

Abstract

Conduction block (CB) is the failure of an action potential (AP) to propagate through an intact axon of a motoneuron. The routinely used methods in clinical practice for CB estimation are based on the comparison of the area and the amplitude of two compound muscle action potentials (CMAPs) elicited with transcutaneous electrical nerve stimulation at sites proximal and distal to the nerve segment in which CB is suspected. The CB estimation obtained with these standard clinical methods is altered by the phase cancellations produced by temporal dispersion of the MUAPs constituting the CMAP. The temporal dispersion is abnormal in subjects with neuropathies that cause important reduction of peripheral nerves conduction velocity by disrupting the myelin sheath (demyelinating diseases). The proposed method is based on deconvolution of CMAPs and provides the delay distributions which convolved with a representative waveform named kernel approximately reconstruct the CMAPs. The slow afterwave of muscle potentials was studied and included in the kernel model and the delay distribution integral was used to estimate the CB.
The method was tested on experimental signals obtained from both healthy and pathological subjects. The pathological group was composed of subjects with Chronic Inflammatory Demyelinating Polyneuropathy (CIDP), with Multifocal Motor Neuropathy (MMN) and with uncertain diagnosis. The results show that the proposed method is stable to temporal dispersion, allowing to obtain CB estimation with a lower confidence threshold with respect to the area and amplitude methods.

Table of Contents

List of Tables

List of Figures

Chapter 1

Introduction

1.1 Electrodiagnostic examination (EDX)

In this thesis, a novel method for the estimation of motor nerve conduction block is presented.
To understand the conduction block (CB) and why its estimation is extremely important, we need to introduce the clinical exams perfomed on patients suffering from pathologies that could cause it.

The electrodiagnostic (EDX) examination provides important informations about the peripheral nervous system (PNS) functionality that complete and extend the findings of a routine neurologic examination. The EDX impression is builded upon the findings of two different clinical techniques, the nerve conduction studies (NCSs) and the needle electrode examination (NEE), that are usually combined in every situation where EDX testing is required [1]. While both parts of EDX are performed quite differently and have individual adavantages and disadvantages, together they provide complementary information of the peripheral nervous system (PNS). The two main goals of the EDX examination are lesion localisation and lesion characterization. Each lesion needs to be localized to the PNS level involved (possibly to the specific functional element) and characterized based on severity, rate of progression and pathophysiological features.

In the most common neuromuscolar diagnostic problems, the NCSs are performed in the first place to assess what muscles will be investigated during subsequent NEE. As previously stated, the complete EDX impression is built upon both exams findings but only the NCSs techniques are able to confirm the presence of various neuropathies and defects of neuromuscolar junction (NMJ) trasmission. It is important to keep in mind that even a complete EDX cannot supplant a meticulous analysis of the patient history combined with a neurologic examination. Besides, the standard NCS assesses only the larger nerve fibers, which are more heavily

myelinated while leaving thinly myelinated and unmyelinated axons unstudied (the myelin utility and the pathologies that disrupt it will be detailed in the following). In the cases of symptoms that are mediated by unmyelinated nerve fibers (e.g. pain or automic disfunction), specialized small nerve fibers testing should be considered. The NCS may be diasgnostically helpful in almost any PNS disorder including disorders of nerve roots, peripheral nerves, muscle, and neuromuscolar junction [2]. Peripheral nerves contain many nerve fibers of different diameters, degree of myelination, and afferent (sensory) or efferent (motor) connections. For this reasons, NCSs are splitted into two major categories which aim to study different kind of nerve fibers:

- Sensory nerve conduction studies
- Motor nerve conduction studies

The sensory NCS assesses the sensory nerve fibers of the PNS from the dorsal root ganglia (DRG) to the most distal group of electrodes (stimulating or recording). The motor NCS, as well as the NEE, assesses the motor nerve fibers of the PNS from the the spinal cord to the muscle fibers that they innervate.

In the following, we will focus exclusively on motor NCSs. That is due to two main reasons:

- The most common primary symptom that brings patients to the electrodiagnostic laboratory or to the clinic is weakness [3]. This specific symptom is certainly caused by an efferent pathway pathology or trauma that leads to ineffective muscle contraction.
- The conduction block, main subject of this thesis, is usually determinated upon the comparison between the compound muscle action potential (CMAP), following electrical stimulation at sites either proximal or distal to the region in which the block is suspected. Motor responses are usually preferred as they are amplified with respect to sensory responses and less susceptible to physiologic dispersion.

1.2 Motor NCS techniques

Motor nerve conduction studies are a fundamental element of the electrodiagnostic examination. They can reflect sever muscle fiber loss, identify axon loss and demyelination and also assess defects of the neuromuscolar junction transmission.

Routine motor NCS techniques involve electrical stimulation of a nerve at distal and proximal sites and the recording of the corresponding motor responses using surface electrodes placed over a muscle supplied by the stimulated nerve.

The external stimulation of a nerve is performed with electrodes or specific stimulators (see Section 1.2.1 for stimulation details). Electrical stimulation produces a current flux exiting the cathod (-) able to, depending on the stimulus intensity and duration, induce a depolarizarion of the stimulated tract, its activation and the propagation of electrical signals along its length. The couple of surface electrodes, active and reference, allows the detection of the motor response: the trasduction of this biologic response in a graphic format (waveform) with basic numerical parameters is commonly performed by the electromyograph.

The motor response is composed of muscle fiber action potentials (APs) and therefore is referred to as compound "muscle" action potential (CMAP). (The generation of the CMAP will be further discussed in Section 1.2.2).
Several parameters are obtained from the recorded responses to assess the number of functionating axons and the speed of the conduction. The results are then compared to normative values, that are usually obtained from literature data in which similar measurement protocols are used. In a similar way, specific electrodiagnostic patterns are identified using various measurements (see Section 1.2.4) that can help discern the nerve pathology nature (i.e. axon loss or demyelinating).
In most EDX laboratories, the upper extremity is mostly studied with median and ulnar nerve stimulation at the wrist and elbow; while the lower extremity is usually investigated with peroneal and tibial stimulation at the ankle and knee (see Figure 1.1 for an example of median motor NCS).

When a peripheral nerve is electrically depolarized, nerve fiber APs are generated and conduct both proximally and distally along its axons, but only the effect of those conducting toward the surface recording electrodes is detected. As depolarization resuls in bidirectional conduction, NCSs techniques are divided in orthodromic (i.e. propagation in the same direction with respect to the physiological direction) and antidromic (i.e. propagation in the opposite direction with respect to the physiological direction). Differently from the sensory responses, which can be collected using both antidromic and orthodromic techniques, motor responses are orthodromically recorded by definition. Therefore, in the following, *orthodromic* will be omitted, as we focus our attention on the motor NCS techniques , in which the recorded APs propagate along the nerve fibers in their physiological direction (from a proximal point to a distal point).

During a routine motor NCS, particular attention is paid to the following questions:

- Is the fastest conduction velocity normal? Refer to Section 1.2.4 for details.
- Is the CMAP normal in size and shape ? Refer to Section 1.2.2 for details.
- Does the CMAP alter in size, shape or duration between stimulation points? Refer to Section 2.1 for details.

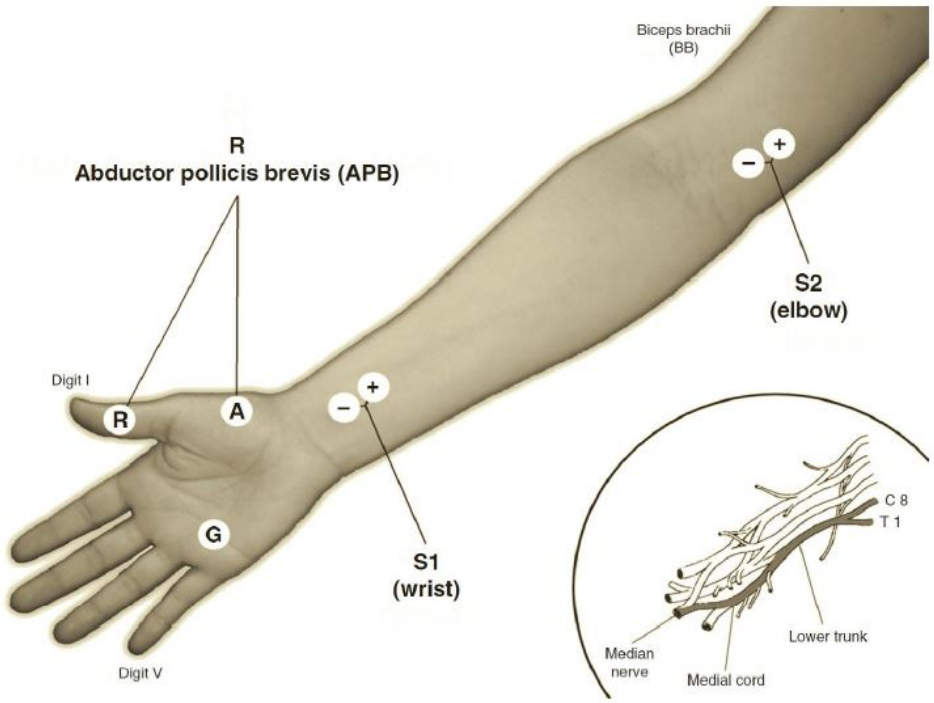

Figure 1.1: Motor NCS of the median nerve. Recording from the *Abductor Pollicis Brevis* (ABP) and stimulating at the wrist (S1) and elbow (S2).

1.2.1 Electrical stimulation

Electrical stimulation finds many applications in a lot of different fields due to its versatility and effectiveness. This kind of stimulation allows to investigate how the neuromuscolar system reacts to a known command. In particular, bypassing the Central Nervous System (CNS), the functionality of the PNS elements can be better investigated. In the routine motor NCSs, noninvasive and low-risk procedures are usually employed, as they are able to evoke a motor response that can be recorded on the muscle while ensuring the lowest discomfort for the patient.

Referring to noninvasive modalities, the most common results to be the transcutaneous electrical stimulation. In electroneurography (ENG) studies, which include the motor NCSs, the above mentioned technique is renamed Transcutaneous electrical nerve stimulation (TENS). This kind of stimulation technique provides for an injection of current in the nerve trunk by means of an external electrical stimulator pressed against the skin.

Electrical stimulators are composed of a stimuli generator and an output stage. The former element is usually linked to an user interface that allows the setting of specific stimulation parameters by the operator and needs a low power supply

(typically a few volts). Stimulation parameters can be optimized by a feedback system. In particular, application-specific parameters can be driven by physiological variables obtained with a sensor and further processed to optimize the performance of electrical stimulation. The output stage needs a high power supply (typically hundreds of volts) and it is directly connected to the skin.

Standard motor NCSs are performed using external handheld stimulators with two metallic prongs, where one is the cathode (negatively charged) and the other is the anode (positively charged). The current flow, produced when the potential difference between the two prongs is applied to the skin, needs to be directed toward the nerve of interest and leakages in the sorrounding tissues needs to be minimized. This requirements are satisfied with small distances between the stimulator prongs (usually 3-4cm) and with skin preparation. To start the stimulation protocol, the handheld stimulator is pressed down against the skin with a pressure sufficient to guarantee localization of the injected current.

The positioning of the stimulator needs to be directly over and along the course of the nerve with the cathode closest to the recording site (Figure 1.1). The stimulation site positioning can be adjusted by using pulses with moderate intensity. One fairly common pitfall that has to be avoided during the stimulation is the so called anodal block. This phenomenon occurs when the stimulating electrodes are reversed and thus the hyperpolarization which take place under the anode results in blocked conduction of the nerve fiber APs. In a routine motor NCS, stimulation is applied at two distinct sites, yielding two separate motor responses (CMAPs). Distal stimulation produces a response that is termed "distal motor response" and, similarly, the proximal stimulation produces a response that is termed "proximal motor response". To properly induce a motor response, all the nerve fibers within the studied nerve have to be depolarized at the same time by the injected current. To guarantee this, the stimulation is initiated at 0 mA and gradually increased until a maximal response is obtained. When the size of the recorded CMAP remains constant despite using higher current, supraximal stimulation is confirmed increasing the intensity by an additional 20%-25%. Thus, supramaximal stimulus generates a maximal response. It is important to avoid submaximal responses as they generate misleading information. In the particular case of in-depth, pennated muscles, the supramaximal intesity should be estimated on the force generated by the muscle rather than on the CMAP amplitude as the latter is strongly influenced by the muscle architecture.

1.2.2 The Compound Muscle Action Potential (CMAP) and its recording

The clinical importance of the CMAP resides in that it allows the study of the PNS efferent nerve fibers without direct involvement of the CNS. In particular,

in a motor NCS, the electrical stimulus applied externally aims to replace the physiologically primed command from the CNS of motor control and therefore needs to effectively induce a depolarization of the nerve trunk innervating a muscle (and all the axons that it comprises). The main requirement to do so is to reach each cell's membrane threshold of depolarization by performing external stimulation correctly (i.e., supramaximal stimulation). Obviously, if the threshold is not reached, no electrical activity is elicited in the nerve fibers of the trunk and thus no motor response can be obtained nor recorded. However, when the membrane threshold is reached, a self-sustaining electrical impulse is generated at the site of stimulation, termed *action potential* (AP).

The motor axons composing the PNS may be myelinated or unmyelinated. As mentioned before, EDX testing (and by extension motor NCS) can study only large-diameter myelinated nerve fibers. Myelinated axons are coated by a lipid-rich substance (*Myelin*) which insulate them and allows a faster propagation of the AP with respect to unmyelinated fibers. The myelin role is fundamental in normal motor function as demonstrated by the consequences of various pathologies that affect it (further discussed in Section 2.1).
The myelin coats the axon in segments rather than forming a single long sheat over the entire length of the axon. The action potential cannot propagate through the membrane in myelinated segments of the axon as they are electrically insulated. Each segment of myelin is generated, in the PNS, by a single Schwann cell and is approximately 1 mm in length. In general, each axon comprises many long myelinated sections (termed *internodes*) separated from each other by short myelin sheath gaps termed *Nodes of Ranvier* (see Figure 1.2). This discontinous structure of the myelinated axon results in saltatory conduction whereby the AP is regenerated at subsequent nodes of Ranvier. In this manner, saltatory conduction allows electrical signals to be propagated for long distances along the axon at high rates without any degradation.

Once the axon terminal is reached, neurotrasmitters are released at specialized regions called synapses. In these regions, the pre-synaptic (motoneuron) and the post-synaptic (muscle) cells communicate with each other via the neurotrasmitters-receptors binding. This chemical synaptic connection is termed neuromuscolar junction (NMJ) and it is the site where the nerve fiber AP is trasmitted to the innervated muscle. The NMJs muscle-related portion is termed motor *end-plate*.

Considering healthy NMJs, a temporal sequence of motor nerve APs is converted into muscle contraction. Each motor nerve fiber arborizes into a large number of terminal nerve branches which correspond to a muscle region termed innervation zone (IZ). The totality of these muscle fibers, linked to a single spinal motor axon, is termed Motor Unit (MU) which represents the basic anatomical and functional unit of skeletal muscles. Each MU has multiple neuromuscolar junctions and one innervation zone (IZ).

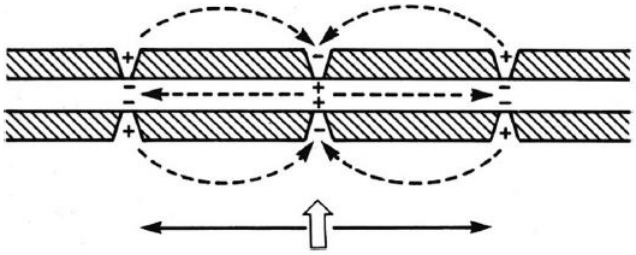

Figure 1.2: Saltatory conduction along a myelinated axon. The myelin sheath effectively insulates the internodal segment with the bare axon at the node of Ranvier, where the current flows between intracellular and extracellular fluid. A local current (*dotted arrows*) induced by an action potential at one node (*open arrow*) depolarizes the axis cylinder at the adjacent nodes on either side, transmitting the impulse in both directions (*solid arrows*).

The CMAP represents the summation of the electrical activity of motor units whose motor axons were depolarized by the stimulus, even though it comprises only the MUs within the pick up territory of the active recording electrode [4]. The contraction of a specific muscle corresponds to a peculiar CMAP and an experienced electrodiagnostician can often identify the motor nerve being stimulated by analyzing its morphology.
Since the 1941, when the first motor response recording technique (by surface electrodes) was developed by Harvey and Masland (i.e. *belly-tendon* technique, further discussed in the following), the CMAP has been used extensively in a wide range of electrodiagnostic applications. Nevertheless, pilot studies about the CMAP electrophysiological determinants started only at the the end of the century [5].
The belly-tendon montage has been adopted by many electromyography (EMG) labs as the usual method of recording compound muscle action potentials (CMAPs). The rationale of this method is that muscles' electrical activity arises at clustering of motor end-plates (muscle belly) and therefore the active electrode (also known as G1) is positioned there. Moreover, the reference electrode (also known as G2) is positioned over the tendon and the ground electrode (which is not always present) is placed between the stimulating and recording electrodes, with the usage of reducing the stimulus artifact.

1.2.3 Factors influencing the recorded CMAP

In this section, a brief description of the most important factors affecting the recorded CMAP shape is provided. These factors should be carefully taken in consideration in each routine motor NCS as they contribution on the waveform

shape may lead to important misinterpretations, which in turn may cause erroneous diagnoses built upon the most common clinical measurements (discussed in details in 1.2.4).

Note that, following the conventional standard in clinical neurophysiology, CMAPs are displayed with negative voltages upward as mentioned in [6] .

- **Recording electrode placement:**

  The shape of the recorded CMAP undergoes important morphological changes when the recording electrode is moved between the innervation zone and the tendon. These changes can be clearly seen considering a muscle in which a well-defined innervation zone can be identified (e.g, biceps brachii). When the electrode is located over the IZ, the resulting CMAP has a biphasic waveform (negative then positive) in which the last phase is usually smaller than the prolonged first one and shows a slow return to the baseline [7], discussed in detail in section 3.2. Moving the electrode towards the tendon, a short and small positive phase (preceding the other two) appears; its amplitude and duration increases as the electrode position approaches the tendon. Over the tendon, the shape become biphasic again with an initial positive phase, followed by a late negative phase.

- **Monopolar vs Bipolar recording:**

  Monopolar detection provides for a single exploring electrode for each recording channel, referred to a stable potential recorded over the subject far from bioelectric sources. The above mentioned belly-tendon recording technique can be classified as monopolar under the strong hypothesis that the reference electrode is electrically inactive. Nevertheless, some studies demonstrated that the influence of the reference electrode on the CMAP configuration is not negligible [8].
  Monopolar detection allows to acquire all the signal information, including the fibre-end effect (i.e., the non propagating component generated when the potential extincts at the tendon). This means that monopolar CMAPs represents the "genuine" potential field present on the skin generated by muscle contraction. However, the monopolar is highly sensitive to the common mode noise (i.e., powerline interference). Another big problem of the monopolar signals is crosstalk, defined as the contribution of a nearby muscle recorded over the muscle of interest. In the context of interest of electrically evoked EMG, the problem of crosstalk could appear when the stimulated nerve trunk innervates various nearby muscles (e.g., adductor pollicis and first dorsal interosseous).
  Noise and crosstalk are the two main reasons behind the extensive usage of other electrode arrangements rather than the monopolar, in particular the

bipolar (single-differential) configuration in which the difference between the potential under two electrodes (usually oriented in the fibers' direction) is computed, removing common components (i.e., powerline noise and end-of-fiber effects). Bipolar recordings allows to greatly reduce the unwanted noise from the system, but their efficacy to reduce crosstalk remains to be validated. The main drawback of the bipolar montage is the "signal cancellation" given by the subtraction of common components in the two recorded potentials which may produce a bipolar CMAP with reduced amplitude. Another negative aspect of the bipolar montage is that it introduces a high-pass filtering on the signal and thus the low-frequency components of the CMAP are attenuated. Noteworthy, crosstalk is thought to impact mostly on the last phase of the recorded potential since its main source is represented by the end-of-fiber signals from nearby muscle.

- **Anatomical:**

  It is important to point out that, even though the CMAP is defined as the summated electrical activity of all motor units in the muscle, only a portion of them contribute to the CMAP in a significative way. To explain the reasons behind this, we have to discuss the anatomycal relation between motoneurons' axons and the muscle units they innervate: Axons with larger diameter are easier to be stimulated and innervate large MUs. Thus, when the nerve is stimulated, larger MUs are recruited before smaller MUs (recruitment order reversed with respect to voluntary contractions where large MUs are recruited at last, when high force levels are required). In addition, the size of the evoked muscle potential is mostly influenced by MUs closest to the recording electrodes due to the attenuation of the electrical field with distance.
  These anatomical properties involve that the assessment of CMAP as a measure of the whole axon pool activation is limited. The spatial organization of the generation sites (i.e., neuromuscolar junctions) and extinction sites (i.e. fiber-tendon junctions) is extremely specific for each muscle within the human body and represent another important anatomic feature that influences the CMAP properties. The spreading of the innervation zone causes higher desynchronization of individual MUAPs which lead to a decreased CMAP size. The spreading of the fiber-tendon junction results in a broadening of the CMAP second phase as the end-fiber effects summate to each other during a longer time interval. [9].

1.2.4 Clinical Measurements

The motor NCS impression is built upon a set of measurements obtained, usually in a very immediate way, from the distal and proximal responses that are compared

with each other and with the laboratory control values. In this section, the most common measurements performed over the motor responses are described.
Note that the features described in the following are related to CMAPs recorded with the belly-tendon technique. Using this recording technique, the CMAPs are biphasic because the active electrode is placed over the motor endplate which means that all the APs are generated directly below it and, thus, no negative preceding phase is present. It is also important to note that, as previously stated, the recording electrode contributes to the waveform morphology (especially its repolarization portion, i.e., the CMAP second phase) and consequently, its placement should be standardized to obtain stable measurements.
For each stimulation site the following parameters are computed: latency, amplitude, duration and area of the CMAP. An example of measurements on a biphasic CMAP is shown in Figure 1.3.

- **Latency:**

  The latency value is marked by the onset of the negative phase (i.e. initial CMAP deflection from baseline) and is measured in milliseconds. Its value cannot be used to estimate lesion severity because it represents only the fastest axons which innervates the earliest muscle fiber to give contribution to the potential recorded by the G1 electrode. In addition, latency usually understimates the motor nerve CV, as it represents three separate processes: (1) the nerve conduction time from the stimulation site to the NMJ, (2) the NMJ trasmission time (about 1ms) and (3) the depolarization time across the innervated muscle.

- **Amplitude:**

  The most common amplitude measure is given by the distance from the baseline to the negative peak and is measured in millivolts. CMAP amplitude reflects the number of muscle fibers (and by extension, of the motor units), that depolarize and thus it may be altered in the presence of anomalous innervation. Since the innervation ratio of a muscle is a constant, the CMAP amplitude is proportional to the number of conducting motoneuron axons (assuming the absence of reinnervation). For this reason, the amplitude is the most important clinical measurement. Nevertheless, among all the NCS parameters, CMAP amplitude appears to have the least reproducibility [10]. The main cause of variability appears to be the inability to reproducibly localize the optimum recording site.
  One common comparison on which the diagnosis is built upon is the decrement between the suspect amplitude value and the controlateral side (see 2.3). It is also important to emphasise that the amplitude stands for the most synchronous MUAPs (primed by the command of the most synchronous motor

nerve fibers) and cannot take in account all the MUAPs that constitutes the recorded CMAP.

- **Area:**

  CMAP area usually is computed as the negative area under curve (AUC), which is the area located under the negative phase of the motor response. Nevertheless, the most information could be extracted from area measurements that consider the waveform along its entire support (i.e. from the onset to the last baseline crossing). However, experimental signals usually present a slow return to the baseline, which makes difficult to identify a distinct end-point. Area measurement cannot be computed manually, thus its computation is assigned to the EMG machine. Negative CMAP area is another measure that stands for the number of muscle fibers and is proportional to the number of motor nerve fibers that depolarize. Area measurements take into account all of the conducting motor nerve fibers.

- **Duration:**

  CMAP duration usually is measured from the waveform onset to the first baseline crossing (i.e., negative peak duration). Another method to measure the CMAP duration is from the initial to terminal deflection back to baseline, but this is less utilized as the terminal CMAP returns to the baseline very slowly making difficult to mark a distinct end-point (see section 3.2 for details about the influence of the slow return to baseline on CMAP duration measurements). Duration reflects the range of CVs of the conducting axons and in particular, it is the time difference between the first arriving MUAPs and the latest arriving ones. It is important to recall the direct proportionality between the duration and the active electrode size.

- **Conduction Velocity:** As mentioned above, the distal motor latency is more than simply the conduction time along the motor axon as it comprises three different processes. Motor conduction velocity (here abbreviated with CV) refers to the propagation time of the fastest conducting axons' APs within the stimulated nerve trunk, which is calculated dividing the distance traveled by the nerve conduction time:

  $$CV = Distance/(PL - DL)$$

  (See Figure 1.4 for a pratical example).
  Therefore, to calculate the motor conduction velocity, without including NMJ transmission and muscle depolarization times, two stimulation sites are required, one distal and one proximal. The distance between the two stimulation sites can be approximated by a tape measure of the surface distance.

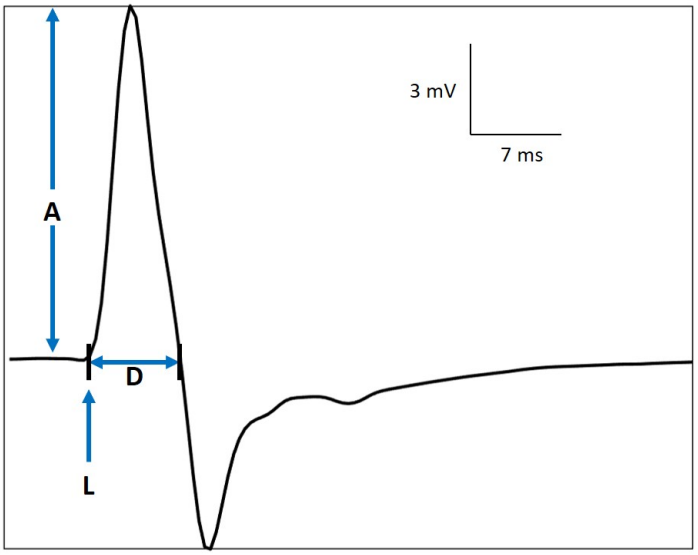

Figure 1.3: Clinical measurements on an experimental CMAP. Latency (**L**) is the time from the stimulus to the initial negative deflection from baseline. Amplitude (**A**) is most commonly measured from baseline to negative peak but can also be measured from peak to peak. Duration (**D**) is measured from the initial deflection from baseline to the first baseline crossing (i.e., negative peak duration). In addition, negative CMAP area (i.e., the area above the baseline) is calculated by the electromyographic machine

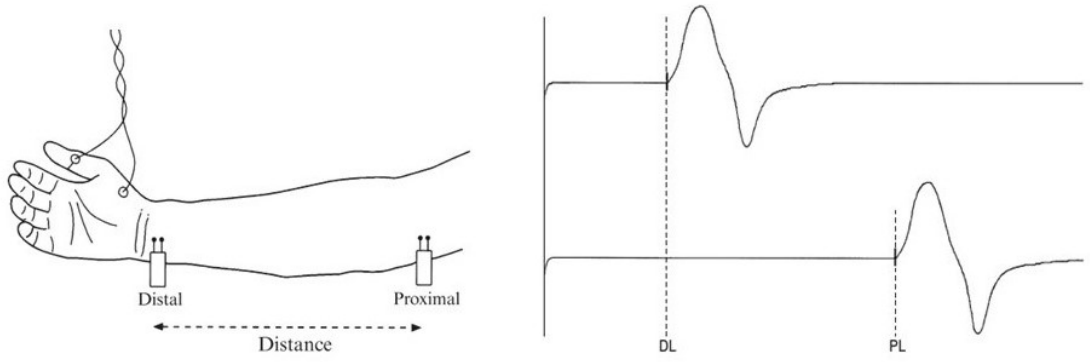

Figure 1.4: Motor conduction velocity (CV) calculation. **Left**: Median motor study. Recording the abductor pollicis brevis activity, elicited by stimulating at the wrist and elbow. **Right**: Compound muscle action potentials (CMAPs) evoked from the supramaximal stimulation: DL, distal latency; PL, proximal latency.

Chapter 2

Conduction Block

2.1 Neuropathic Lesions

Motor nerve conduction studies can assess several abnormalities which depend on the underlying pathology. The pattern of abnormality is the result of disorders affecting different portions of the motor control pathway, starting from the anterior horn cell (from which the motoneuron is derived) to the muscle. In this section we will focus on the nerve pathologies, usually termed peripheral neuropathies, that are divided into those that affect the axon and those that affect the myelin sheath, named primary axon loss and primary demyelination, respectively .

The differentiation between primary axon loss lesion and primary demyelinating lesion is one of the main diagnostic goals of NCSs. The EDX provider must recognize the manifestations associated with the pathophysiology resulting from the nerve fiber disruption since they have both diagnostic and prognostic implications. The following description points to show the electrodiagnostic patterns of axon loss and demyelination while highlighting that the pathological mechanisms that lead to conduction block are mostly caused by demyelinative processes. [11].

2.1.1 Axon loss

Axon loss lesions are the most common pattern identified during motor nerve conduction studies.
When an axon is disrupted, its distal portion is no longer connected to the cell body and undergoes a degenerative process called *Wallerian degeneration*. The Wallerian degeneration is not an istantaneous process and affects mostly the nerve fiber regions distal to the lesion. As motor nerve axons are lost, the corrispective muscle fiber APs are not generated, which in turn leads to a reduced amplitude and area of the recorded CMAP [1]. Note that the inverse relation is not necessarily true, which means that reduced CMAP amplitude (or area) does not imply axon

loss (see Section 2.1.2).
From a clinical point of view, since the APs are unable to cross the lesion site, loss of fiber contraction (weakness) and loss of sensation (numbness) are present in the patient if the motor conduction or the sensory conduction are interrupted, respectively. Once the degeneration process is complete (e.g., after 8 days in the case of an acute transection of the median nerve), all the distal portion of the axon becomes unable to conduct any AP and thus, the proximal (stimulus applied above the lesion) and distal (stimulus applied under the lesion) motor responses are identical. The APs cannot propagate across the proximal lesion, while in the distal segment no APs are generated regardless of the stimulation intensity. Each peripheral nerve contains a normal distribution of conduction velocities, in which the highest is related to the largest nerve fibers. For this reasons, the axon loss pattern depends on which fibers are disrupted and their conduction velocity.

The amount of axonal loss is usually assessed by comparing the amplitude of a recorded potential with the controlateral (asymptomatic) side or with a normal control value. If the largest and fastest conducting axons are intact, conduction velocity and distal latency appear normal. Note that mild slowing of both conduction velocity and distal velocity may occur if the fastest axons are lost. However, marked slowing does not occurr, as myelinated fibers simply cannot propagate under a certain velocity (which depends on the specific nerve trunk, for example the median nerve conduction velocity range is usually $35m/s$ to $65m/s$). This is a main difference with respect to demyelination, in which the demyelinated axons conduct at velocities much slower than the physiologic lower value.
In the majority of cases, axon loss lesions lead to a random drop out of fibers (see Figure 2.1).
To sum up, the typical pattern associated with axon loss is one of reduced amplitudes and almost totally preserved conduction velocities and latencies (see Figure 2.2 for details).

2.1.2 Demyelination

Demyelination is the main pathophysiologic manifestation of demyelinative disorders and/or of Schwann cell disfunction (e.g., diphteria). Demyelination resulting from dysfunction of the myelin sheat is seen mostly in entrapment or compressive neuropathies. Other conditions which may lead to myelin damage are also possible, some of which are genetic, some toxic, and some are due to immunologic system disfunction. The totality of demyelinating neuropathies (a list of the most common ones is provided in the following) is divided in hereditary and acquired. This dichotomy is defined upon the way in which the nerve fibers suffer the demyelinative process:

- HEREDITARY NEUROPATHIES: demyelination affects the nerve throughout its

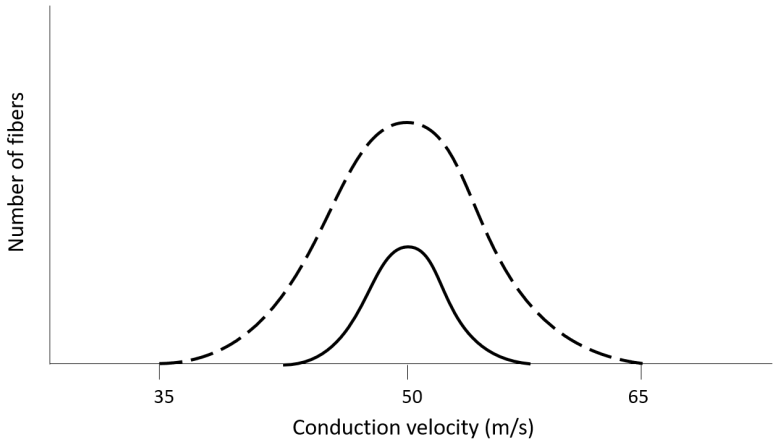

Figure 2.1: Median nerve axon loss pattern with random dropout of fibers due axon loss. Dashed line: healthy CVN distribution, solid line: pathological CVN distribution. This is a more typical pattern of axon loss than the extreme cases in which a few of either the fastest or slowest normal fibers remain intact after axon damage.

length in an uniform fashion. In this case, little differences among different members of the same family and from one nerve to another in the same patients are present. This kind of pathology leads to uniform conduction slowing but no conduction block is present.

- ACQUIRED NEUROPATHIES: demyelination affects different nerve segments disproportionately, resulting in conduction block in certain parts of the nerve (focal demyelination). In this case, asymmetrical abnormalities and increased temporal dispersion are expected in patients. This group of pathologies is the one of interest.

The thinning (or even the total absence) of myelin sheath in a nerve segment increases the internodal capacitance and conductance, leading to a loss of current. The current is then non sufficient to activate the subsequent node of Ranvier (see Figure 1.2) , this failure of activaction results in conduction block. Going into detail, demyelinating neuropathies include Acute inflammatory demyelinating polyradiculoneuropathy (AIDP, the most common variant of Guillain–Barré syndrome), chronic inflammatory demyelinating polyradiculoneuropathies (CIDP), Multifocal motor Neuropathy (MNM),myelomatous polyneuropathies, hereditary

motor sensory neuropathy type I, metachromic leukodystrophy, Krabbe's leukodystrophy and Niemann-Pick disease [12].
As stated in 1.2.2, myelin is fundamental to the axon's saltatory conduction. Therefore, pathologies that disrupt it can cause either markedly slowed or blocked nerve conduction, depending on the myelin disruption extent. When the amount of myelin loss is limited, slowing of the nerve fiber APs occurs. It can be uniform (i.e., all the fibers are slowed to the same degree - related to hereditary neuropathies) or nonuniform (i.e., different fibers are slowed to a different degree - related to acquired neuropathies). The nonuniform conduction slowing results in pathologically dispersed CMAPs by means of abnormal temporal dispersion (whose effects on the CMAPs will be discussed in detail in 2.4), in which the constituent MUAPs are separated in time proportionally to the degree of conduction slowing in the axons (Figure 2.2). Nevertheless, slowing of conduction leads to little, if any, clinical symptoms, as all the electrical impulses arrive to the target muscle. Peripheral nerve demyelination needs to be assessed with specific criteria. Research criteria include latency prolongation $> 125\%$ and conduction velocity slowing to $< 80\%$ of normal values [13].
When the amount of myelin sheat disruption increases, the APs eventually become unable to cross the lesion. In this situation, the demyelinated portion of the axon actually "blocks" the nerve APs conduction toward the neuromuscolar junction. This condition is known as *demyelinating conduction block* (DMCB or simply CB, as it will be addressed in the following) and correlates best with the degree of weakness of patients with demyelinating diseases.
To sum up, demyelinated nerve fibers characteristically show:

1. conduction block

2. abnormal temporal dispersion

Noteworthy, if the proximal and distal stimulation site are erroneously positioned on the same side of the lesion, the lesion is not discernible (Figure 2.2, right panel, second-to-last plot). It is important to point out that, during the first 3 days of the nerve insult due to Wallerian degeneration, distally evoked motor responses have normal amplitude while proximally evoked ones have reduced amplitude. In this unique situation, termed *pseudo-conduction block*, the only way to discern between the CB (pattern typically associated with demyalination) and the acute axon loss lesion is to repeat the measurement after 1 week. In a true demyelinating lesion the conduction block pattern will persist, while in the axon loss lesion both CMAP amplitudes will be reduced (meaning that the wallerian degeneration is complete).

In addition, mixed patters of demyelination and axon loss are fairly common. This is due two main factors:

1. electrophysiological features of demyelination are developed in axon loss processes as a reflection of nerve regeneration.

2. progressive demyelination is usually associated with damage to the underlying axons.

An example is the diabetic polyneuropathy, which is an axon loss disorder whose electrophysiologic signature comprises some sign of demyelination.

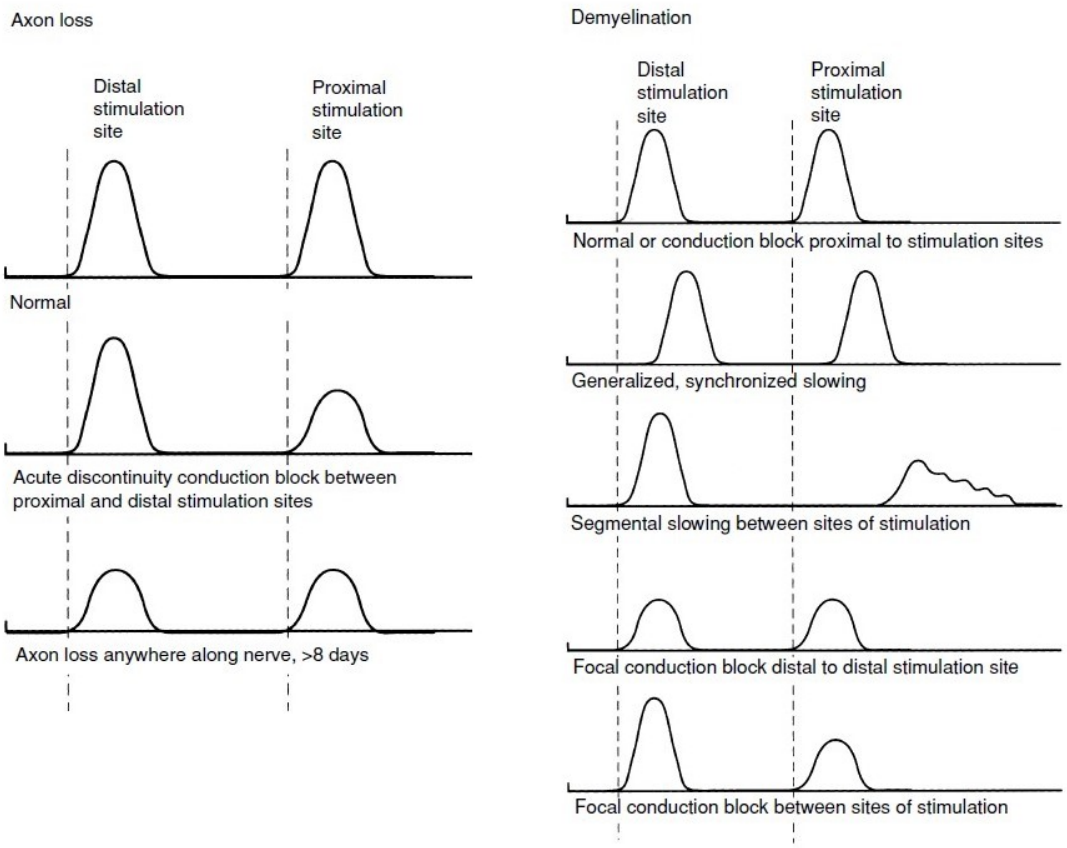

Figure 2.2: Electrodiagnostic patterns of axon loss and demyelination. Only the first phase of an ideal CMAP is shown. **Left**: CMAPs with various axon loss lesions. **Right**: CMAPs with various demyelinating lesions. The first waveform in each line results from distal stimulation, and the second waveform results from proximal stimulation.

2.2 Model of CB and its location

In the previous sections, a brief description of the axon loss and demyelination patterns of abnormality has been provided, ending with the definition of the demyelinating conduction block. Here, an anatomical model of CB and a review of the common clinical methods used to estimate it are discussed.
This review aims to define the main problems and limits of the currently most used clinical techniques to estimate CB during NCSs and play an introductive role to the developed advanced method for CB estimation which will we be described in detail in Chapter 3.

Conduction block is defined as the failure of an AP to propagate along one axon which remain structurally intact. Following the definition, conduction block is a potentially reversible abnormality. In the majority of cases, CB is a transient phenomenon and recovery is possible. However, there are several situations in which CB becomes a persistent cause of weakness. Mostly because of these chronic conditions, CB needs to be reliably identified and quantified to develop effective therapeutic procedures. As previously stated, the most common cause of demyelination and in turn of conduction block are the compression neuropathies in which a segment of the nerve is mechanically compressed. These disorders are readily identifiable and usually respond to surgical therapy. Nevertheless, in this thesis, the attention will focus on the chronic multifocal demyelinating neuropathies, which leads to the most complex motor responses (i.e. very dispersed and altered CMAP waveforms). In these pathological conditions, demyelination is usually a segmental and patchy process, which causes conduction block along a variable number of motor nerve fiber within the stimulated nerve trunk, as shown in Figure 2.3.

Regardless of the underlying pathology, demyelinative lesions usually comprise both conduction block and temporal dispersion.
From a clinical point of view, the distinction between these two physiologic alterations is important because it defines how the neuropathy will be managed. In particular, while temporal dispersion may be present without weakness, conduction block always lead to weakness and therefore its recognition has a big value in making therapeutic decisions.

Figure 2.4 shows the importance of the stimulation sites on the recorded CMAPs amplitude with respect to the lesion position. The usual situation, in which the lesion is correctly identified, corresponds to conduction block between the distal and the proximal stimulation sites (Figure 2.4,**Middle**). In this situation, the proximal CMAP is expected to have decreased amplitude. On the other hand, stimulation sites may be erroneously placed on the same side of the lesion, either distally or proximally, leading to difficult assessment of conduction block presence. (Figure 2.4, **Bottom** and **Top**, respectively).

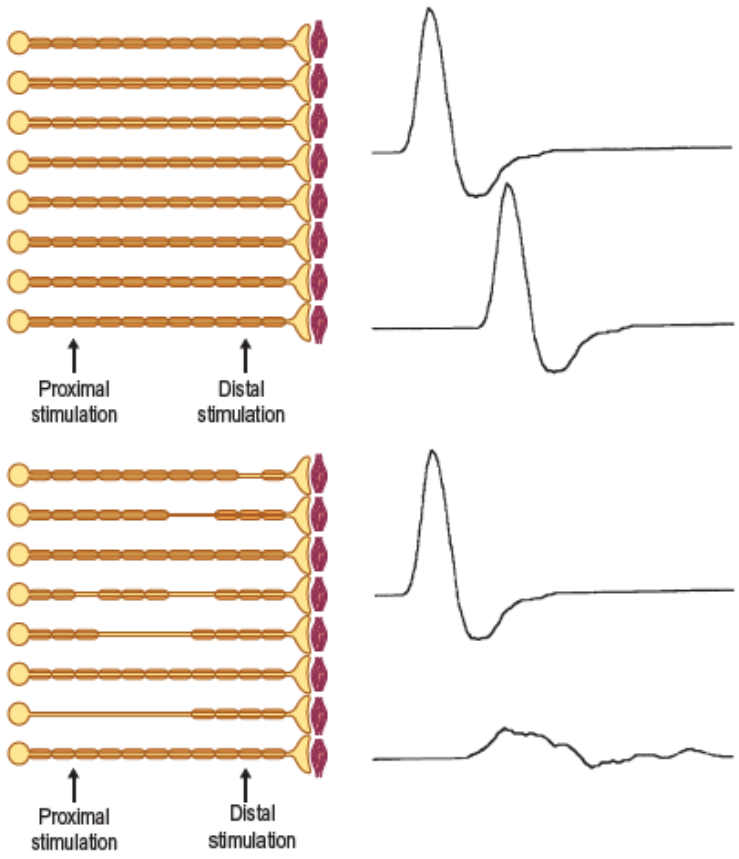

Figure 2.3: Model of CB. **Top**: Normal nerve in which all the motor axons are myelinated. The CMAP waveforms are similar when comparing distal and proximal stimulation sites. **Bottom**: Nerve with multifocal demyelination, the proximal CMAP drops in amplitude and area and becomes abnormally dispersed.

2.3 Classical methods for CB estimation

At the current time, several methods have been proposed to estimate the conduction block. The great majority of them is based on quantitative comparisons between the CMAPs obtained following distal and proximal stimulation (see Figure 2.3 for an example of CMAPs obtained in a control subject and in a pathological one). In demyelinating lesions, the crucial question that needs to be addressed is how much of a drop in the CMAP size is needed to properly identify a conduction block. Here, the two most used clinical methods (of the amplitude and area) are briefly described, to provide a reference for the advanced new method described in the next chapter. The common theoretical basis on which these methods rely, is that CMAP

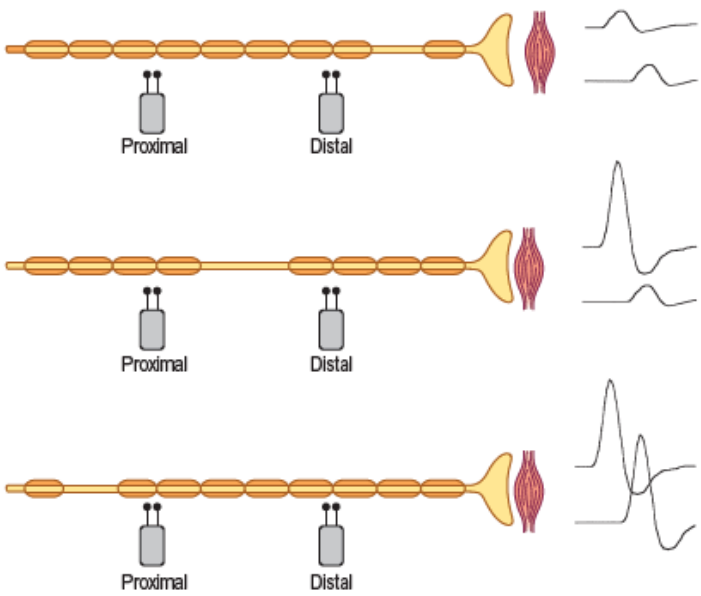

Figure 2.4: Conduction block location. **Top**: Decreased CMAP amplitudes at both distal and proximal stimulation sites, misleading axon loss pattern. **Middle**: Decreased CMAP amplitude at proximal stimulation site, common CB pattern .**Bottom**. Same CMAP amplitude among the two stimulation sites, misleading normal axonal conduction pattern.

measurements (i.e. amplitude and area) are related to the number of active MUs and in turn to the conducting motor axons. Therefore, the assessment of changes in the value of these parameters between the proximal and the distal CMAP is the common clinical pratice to quantify the severity of the CB. The severity of CB is defined as the number of axons whose conduction is interrupted with respect to the total number composing the stimulated nerve trunk (usually expressed in %). Refer to Section 1.2.4 for details about the measurements described in the following.

Method of the amplitude

This method simply compares the amplitude of the two CMAPs recorded following a proximal and distal stimulation. Since the conduction through some axons is interrupted, the corrispective MUs are not elicited, leading to an amplitude reduction. Thus, an estimation of the severity of the CB is given in terms of the following amplitude ratio

$$CB_{Amplitude} = \frac{\max(v^{prox}(t))}{\max(v^{dist}(t))} \tag{2.1}$$

Where $v^{prox}(t)$ and $v^{dist}(t)$ are the proximal and distal CMAPs, respectively. The amplitude of the CMAP is assumed to be related to the number of active MUs. Thus, the decrease in amplitude is used to estimated the number of MUs affected by the CB.

Method of the area

In this method, the severity of the CB is estimated by comparing the areas of the two CMAPs recorded following proximal and distal stimulation. An important factor that affect this method is how the area is computed. The most common measure is the negative area (area of the first phase of the CMAP) as the second phase of the CMAP is usually determined by the summation of end-of-fiber components generated at the extinction of the muscle fiber APs at the MTJs (i.e. muscle-tendon junctions). Nevertheless, here is reported the general formula in which all the CMAP waveform is considered for area measurements, considering all the electrical activity generated by the muscle contraction (i.e, both phases are considered)

$$CB_{Area} = \frac{\int_{t_{A1}}^{t_{A2}} |v^{prox}(t)| dt}{\int_{t_{B1}}^{t_{B2}} |v^{dist}(t)| dt} \tag{2.2}$$

where the integrals are computed on the supports of the two waveforms.
The method of the area has been proven to be more reliable than the amplitude's in quantifying conduction block in the wide range of peripheral neuropathies that cause it [14]. The method of the area provides more information than the method of the amplitude especially when contrasting conduction block and temporal dispersion. Noteworthy, area measurements are more stable to changes in the active electrode placement, which is a consistent issue when the amplitude is used in clinical practice. However, area reduction of the proximal CMAP may be related to physiological mechanisms other than conduction block, as suggested by [14], in which area reduction was observed in groups of normal subjects.

2.4 Problems of classical methods for CB estimation

At this point, the physiological meaning of conduction block and its clinical consequences have been discussed. Considering a single axon, the detection of conduction block and its evaluation is simply performed by recording invasively the AP propagating along a certain segment. However, the assessment of conduction block in a nerve composed of many axons (which is the common situation of clinical relevance) is a more difficult task.
This difficulty is dictated by the CMAP, which is produced by the spacial and

temporal summation of many biphasic (if the belly electrode is place above the endplate) MUAPs, which are the result of axonal APs volume conduction throughout the innervated muscle. This summation process results in phase cancellations (i.e., negative phases of some MUAPs cancelling out positive phases of other MUAPs) and therefore the amplitude and area of the recorded CMAPs may be less than the arithmetic sum of the individual potentials. The spatial summation effect can be considered equivalent in both normal and neuropathic conditions, as it is related to a constant muscle geometry made of healthy muscle fibers (myopathy is not present).
On the other hand, temporal dispersion within a motor response is mainly determined by the length of the studied nerve segment and by the range of conduction velocities within the specific nerve trunk. Additionally, duration of the negative phase and the amplitude of each MUAP both have influence on the resulting phase cancellation. In particular, shorter duration responses are more susceptible to dispersion than longer ones and smaller amplitude responses are more susceptible to decrement than the longer ones.

Temporal dispersion describes the relative desynchronization of simultaneously evoked components of a compound action potential due to different rates of their conduction. This dispersion results in changes of amplitude, area, duration and Fourier spectra of the CMAPs when comparing proximal with distal nerve stimulation [15]. This is the main problem of the classical methods based on the comparison of CMAPs waveform features like area and amplitude, given that their changes between the two recorded CMAPs cannot be divided between those caused by temporal dispersion and conduction block. For this reason, the above mentioned classical methods may fail to be diagnostically efficient in situations where both conduction block and abnormal temporal dispersion are present.

Notably, a certain degree of temporal dispersion between normal MUAPs is always present (termed *physiologic dispersion*) due to the normal range of CVs in the peripheral nerves, which means that all the MUs are not simultaneously activated even with distal stimulation. In addition, the temporal dispersion depends on the nerve segment length: as the distance between the two stimulation sites increases (referred to as *conduction distance* in the following), the APs become more dispersed in time. Because of this, motor NCSs are usually preferred to sensory NCSs since the muscle potentials are less susceptible to phase cancellations, given their longer duration and higher amplitude, and thus much longer segments can be studied during motor NCSs than sensory NCSs.

However, it is in the presence of demyelination, in particular when conduction is slowed nonuniformly in a populations of axons, that temporal dispersion and relative phase cancellations increase their effect on the recorded CMAPs. Several simulation studies addressed the impact of both CB and temporal dispersion on the detected CMAPs: [16], [17] . In particular, CMAP area has been demonstrated

to fall up to 50% and the amplitude to an even higher extent, exclusively because of temporal dispersion and phase cancellations, without any condution block on the simulated nerve fibers [18]. It is important to note that these area an amplitude reductions meet the today accepted criteria for conduction block. Figure 2.5 is extracted from [18] and shows how impactful temporal dispersion can be on the recorded CMAPs. The cited paper proposed that a criteria of more than a 50% drop in area between proximal and distal CMAPs should be used to define conduction block to cope with the temporal dispersion effect.

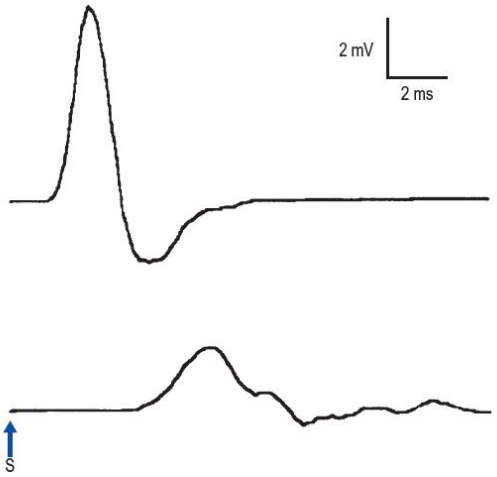

Figure 2.5: Temporal dispersion effect on CMAPs. The only alteration is an abnormal proximal CV distribution. Thus, the drop in amplitude is entirely due to abnormal dispersion from a demyelinating lesion. The blue arrow marks the stimulation onset. Note that the amplitude and area are both greatly reduced, matching the common clinical thresholds for CB assessment, even though no CB is present.

To conclude this review, another factor should be taken in account (again, explained in detail using simulated signals in [18]): the large motor units (innervated by the fastest conducting axons) have a great impact in determining the configuration, amplitude and area of the CMAP. Hence, the greatest phase cancellation effects are due dispersion of these big MUs activity, which produce high amplitude MUAPs. Thus, quantitation of CB and temporal dispersion based on CMAP amplitude and area should be performed knowing which subpopulations of axons are affected. Unluckily, these informations can be obtained only with complex invasive techniques and are usually unknown during motor NCSs.

For all the above described reasons, a new method to estimate conduction block based on deconvolution of CMAPs is described in the next chapter.

Chapter 3

Advanced method for CB estimation

In this thesis work, a novel method for CB estimation is developed, based on the deconvolution of CMAPs. The theoretical and practical basis of the method were provided by Professor Luca Mesin's and its innovative paper [19], with the main goal of tuning the algorithm for its applicability to pathological patients. In fact, there is great distinction between pathological subjects and healthy subjects, in terms of motor responses. This differences needs to be taken into account to obtain a new, reliable method for CB estimation. The experimental data acquired on pathological subjects was provided by Dr. Dario Cocito and his team.
The CMAPs deconvolution provides both the delay distribution and the kernel (representative MUAP) that reconstruct approximately the data. The great advantage of this method with respect to Amplitude and Area methods is that to be ideally insensitive to temporal dispersion. The delay distributions would allow, in ideal conditions, to estimate reliably the CB presence and its severity, compensating for phase cancellations. The kernel shape is optimized to have the minimum error in reconstructing both the CMAPs, when convolved with the estimated delay distributions.

3.1 Mathematical model and notations

As described in detail in 1.2.2, a CMAP is the sum of all the MUAPs elicited in the muscle by electrical stimulation of the peripheral nerve that innervates it. The general mathematical model of a CMAP is the following:

$$v(t) = \sum_{n=1}^{N} v_n(t - \tau_n) \tag{3.1}$$

where $v(t)$ is the acquired CMAP, N is the number of active MUs producing it and v_n is the general waveform of the nth MUAP with delay τ_n. The delay τ_n stands for the AP's time of propagation along the motor axon innervating the nth MUAP. Each nerve has a specific nerve conduction velocity (CVN) range (see Figure 2.1 for an example), which is reflected on the MUAPs delay distributions. The AP travels from the stimulation site to the end-plate, where it induces fiber contraction by priming a trasnmembrane current transient. As previously described , this mechanism is mediated by the neuromuscolar junction (NMJ) that introduces a specific time delay termed *synaptic delay*. The synaptic delay is assumed constant for all the NMJs within the innervated muscle and thus not considered in the delay distributions.
Each MUAP shape, indicated by $v_n(t)$ in (3.1), depends on the volume conductor properties (i.e., geometry and conductivity), on the position of the nth MU's fibres and their conduction velocity (CVM). Nevertheless, given the high number of unknowns that needs to be determined in order to obtain the delay distributions (N, τ_n, $v_n(t)$), some assumptions needs to be made. Above all, we assumed that all the MUAPs $v_n(t)$ could be represented by a specific common wave shape, referred to as kernel, and differ only in the amplitude:

$$v(t) \simeq \sum_{n=1}^{N} A_n K(t - \tau_n) \tag{3.2}$$

where A_n is the amplitude of of the nth MUAP, $K(t)$ is the kernel and τ_n its delay. In this way, each MUAP is represented by a kernel that has a specific amplitude, reflecting the location and dimension of the MU generating it, and a specific time delay, reflecting the CVN along the axon innervating that specific MU. It is important to note that the MUs are not innervated in the same point and thus also the time delay due to propagation of the action potentials along the muscle fiber is included in the delay τ_n in model (3.2).
The delayed function can be written as the deconvolution of a waveform with a Dirac delta. In this way, the model becomes:

$$v(t) = K(t) * \sum_{n=1}^{N} A_n \delta(t - \tau_n) = K(t) * x(t) \tag{3.3}$$

where $x(t)$ is the delay distribution, written as the sum of Dirac delta functions delayed in time and scaled in amplitude.
Finally, a perturbation term is included in the model, taking into account the always present noise in experimental data and the strong approximation that the MUAPs need to be quite similar in shape.

$$v(t) = K(t) * x(t) + n(t) \tag{3.4}$$

Note that solving this problem is difficult for two main reasons:

1. Both the kernel and the delay distribution are unknowns.

2. It is an inverse problem, the cause is computed given the effect.

The details of how the deconvolution problem is solved numerically are described in 3.3. Nevertheless, we must firstly focus on the shape of a CMAP and its various portions, which are related to important electrical events that take place in the muscle.

3.2 The slow afterwave in muscle action potentials

The deconvolution method is based on the definition of a kernel, representative of the common shape of MUAPs that make up the CMAP. The kernel estimation is performed blindly (blind econvolution) but its shape must be substantiated on the MUAP electrogenesis (i.e, the stages of evolution of the potential field during a discharge of a MU) that is fundamental to understand how a MUAP and a CMAP should look like in our case of surface recordings (which usually refer to small muscles, like *abductor pollicis brevis*).
For this reason, the CMAPs' shapes acquired from both healthy and pathological subjects were studied in detail and compared with important research papers results in order to understand how, starting from the mechanisms underlying the MUAP generation, the best kernel possible could be obtained.

We must start by saying that the CMAP formation has been studied with the main goal of modelling its slow return to baseline in the kernel, which in the following will be named slow afterwave (SAW) using the name given to it by Lang et al. in 1973. This component has been studied since the late 90s, however it has received very low consideration in the clinical field applications. Its importance depends on the purposes for which the CMAP is analyzed. In the field of electrodiagnostic it should be carefully taken in consideration because it can contribute as much as the MUAP (or CMAP) total duration.
In this regard, the CMAP duration has been proven to be a valuable parameter in the diagnosis of demyelinating neuropathies (e.g., CIDP). In the research reports [20] and [21], the distal CMAP duration was reported as an useful index for the detection of distal myelination since it also takes into account the temporal dispersion while the distal latency can highlight only the conduction slowing of the fastest fibers. In both of these works, the duration measurement didn't include the final phase of the potential, which returns to the baseline without a distinct endpoint.
Figure 3.1 shows two experimental CMAPs, obtained by stimulating two different subjects and two different nerves, in which the slow afterwave is clearly visible.

It is evident that the slow return to the baseline makes it difficult to identify an endpoint in both the showed CMAPs due to its asymptotic behaviour. In Figure 3.1 (B) a CMAP recorded from a patient with chronic inflammatory demyelinating polyneuropathy (CIPD) is shown: in that case the slow afterwave has higher relative amplitude with respect to the healthy signal making its contribution higher on the CMAP waveform. This is due to, among other factors that will be described in the following, the temporal dispersion affecting the pathological CMAP generation, causing the separation of the first phase in more than one deflection across the baseline. For this reason, in the pathological cases, a revised definition of CMAP duration was used, taking into account the temporal dispersion caused by conduction slowing in demyelinating conditions: the duration was defined as the time period from the first negative deflection of the CMAP to return to baseline of the last negative deflection of the CMAP. Further, the CMAP area should be computed in the same way when the first phase is dispersed and more than one baseline crossings (negative to positive) are present.
This area computation was used in this work.

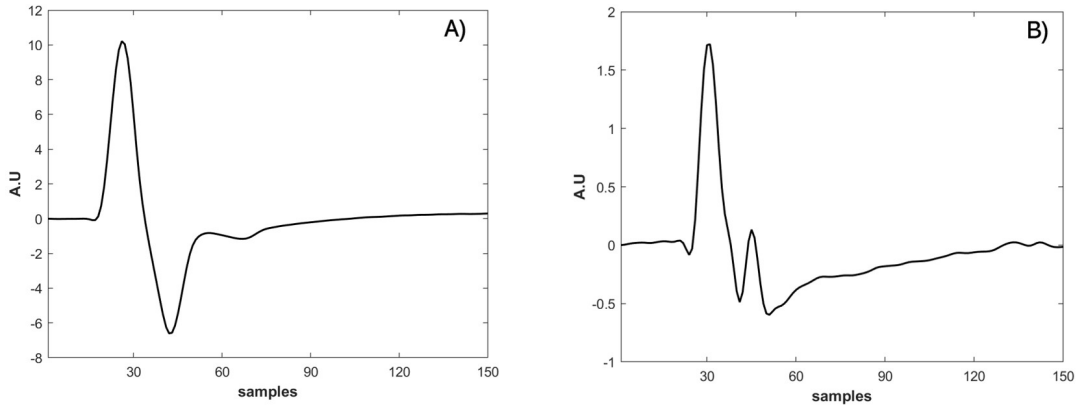

Figure 3.1: Proximal CMAPs in which the slow return to baseline or slow afterwave (SAW) is clearly visible. The x-axis corresponds to 75 ms. **A**: Proximal CMAP acquired from healthy subject, ulnar nerve stimulation . **B**: Proximal CMAP acquired from pathological subject with CIDP, median nerve stimulation.

Several factors influencing the CMAP shape has been previously described in section 1.2.3 and now we can focus on the slow afterwave description while keeping them in mind. To properly study this component generation, a new study should be necessary, requiring complex simulations of MUAPs and CMAPs starting from the intracellular action potential (IAP). Since this thesis goal wasn't to study the CMAP parts (and in particular the slow afterwave) with mathematical models, we derived the useful information about the IAP and the simulations from research

articles. Nevertheless, the comparison between the provided experimental signals (CMAPs) and the literature description of the slow afterwave led to a good solution in the kernel estimation which significantly improved the method performances on patients.

Since the motor NCSs are mainly performed over the hand muscles and the experimental signals on which the deconvolution method is tested are mainly recorded from thenar and hypothenar eminences, in the following our attention will be focused on CMAPs recorded over the hand. To be able to understand the different signals that can be recorded on the skin surface, we need to briefly describe how the CMAP potential field evolves in time. The CMAP is seen as a record of the sequence of electrical events that take place in the muscle. McGill and Lateva produced extremely important papers on this topic, which were the theoretical foundation of our solution to include the slow afterwave in the kernel model.
The CMAP field is the sum of individual MUAP fields, that are dispersed in time (due to differences in nerve-impulse arrival times) and in space (due to differences in end-plate locations). Nevertheless, these dispersions are small when hand muscle are considered. For this reason, both the CMAP and the MUAP evolution in time can be represented with the stage shown in Figure 3.2, reproduced from [22].

The electrical activity of the muscle fibers is divided into four stages, which are present in both voluntary and evoked MU discharges:

1. initiation
2. propagation
3. termination
4. slow repolarization

The surface-recorded signals, that we want to describe, are the result of the electrical events detected over several centimeters, including the entire length of short muscle fibers (which make up for the hand muscle). This means that all the stages of electrical activity above introduced affect the surface-recorded signals of interest. The terms used to describe the evolution of the potential field in the following are derived from [7], in which the anatomical and electrophysiological determinants of the thenar CMAP were described for the first time. The initiation stage refers to the depolarization of the end-plate region (Figure 3.2**a**), in which the trasmembrane current can be modeled by a quadrupole source (+ - - +) which produces a negative potential field over the end-plate, referred to as *initial standing wave*. During the propagation stage, the stationary quadrupole is splitted into two traveling quadrupoles which travel toward both muscle fibers terminations (Figure 3.2**b**) . These two waves are termed *traveling waves*. On a surface recorded

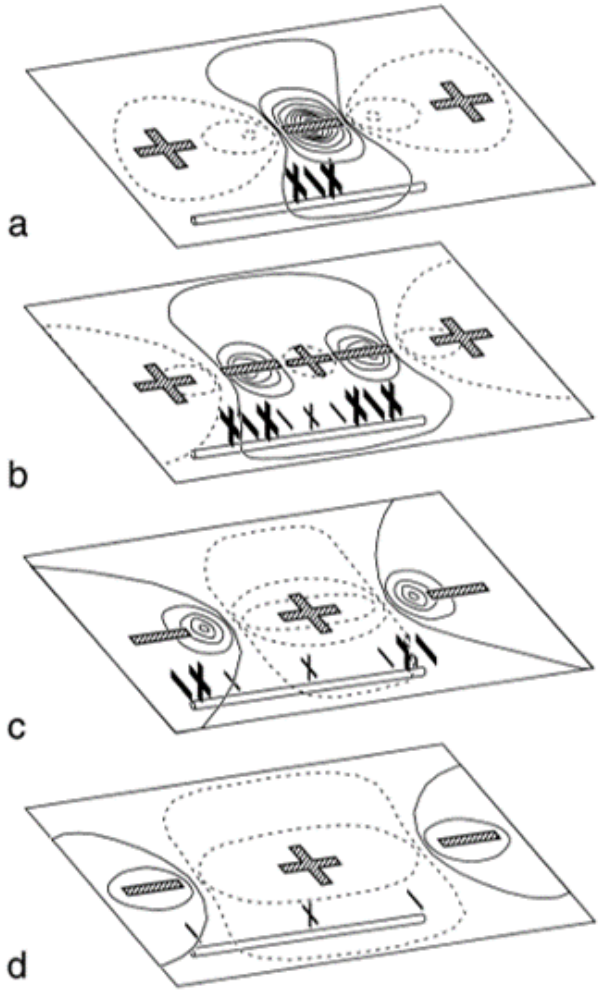

Figure 3.2: Four stages of evolution of the extracellular potential field. (**a**) initiation, (**b**) propagation, (**c**) termination, and (**d**) slow repolarization. The transmembrane current sources along the muscle fibers are represented by the filled '+' and '-' symbols: the larger symbols correspond to the waves of excitation, the smaller ones to the slow repolarization. The source configuration ' + - +' is called linear quadrupole (indicated by ' + - - + ' in the text) and the source configurations '+ - ' and ' - + ' are called dipole sources.

potential field, their effect is limited to extend the initial standing wave duration (forming the negative peak of the CMAP). Notably, the quadrupole source can be regarded as the sum of a leading (- +) and a trailing (+ -) dipole source.

After the passage of the traveling wave that excites the muscle fiber membrane, the muscle undergoes repolarization in two phases. The first 80% of repolarization takes place within 1ms after the depolarization and the remaining 20% takes place over a period lasting 10ms or more, referred to as *slow repolarization phase*. The slow repolarization phase is referred to as the *negative afterpotential* of the intracellular action potential (IAP) and is thought to be due slow ionic processes in the T-tubular system (see Figure 3.3). The termination stage refers to the time during which the depolarized zones reach the ends of the muscle fibers. At this stage, the quadrupole sources become two stationary dipoles as both the leading dipoles disappear when they reach the ends of the fibers. The fields generated by these stationary dipole sources are termed *terminal standing waves* and represented with filled symbols in Figure 3.2**c**.

Finally, the slow repolarization stage (Figure 3.2**d**) refers to the time after the termination of the action potential when the entire muscle is undergoing the second slow stage of repolarization. The field decrease at the same rate as the negative afterpotential of the IAP and has a spatial configuration very similar to the terminal standing wave.

Several ideas were tested in this thesis to properly cope with the slow afterwave affecting the experimental signals from which we wanted to obtain e reliable CB estimation with the deconvolution method. Several efforts were made in the directions of signal truncation and signal smoothing. This attempts were based on the hypothesis that by removing the slow afterwave, the CMAP could be well reconstructed using exclusively Hermite polynomials and their linear combination optimization (see section 3.4). After several attempts we decided that this asymptotic component with which the CMAPs return to the baseline was too critical for the deconvolution method since no CMAP windowing or truncation methods allowed to obtain good performances. For this reason, we decided that the best solution was to consider this component in the kernel. Several mathematical models, that here are not described, established that the surface-recorded muscle signals should be affected by the slow second stage of repolarization of the muscle-fiber membrane (i.e., negative afterpotential) and contain a slow component corresponding to it. Obviously, the main requirement to include this component in the kernel, was that it had some physiological origin and it was not due some artifactual components. This hypothesis has been tested by Lateva and McGill in [23] and their results will be briefly reported and commented on the basis of the signals at hand in the following. In particular, it was demonstrated that the slow afterwave in muscle potentials is a manifestation of the IAP negative afterpotential.

But what is the IAP negative afterpotential? It is the slow repolarization phase that follows the spike that can last for tens of milliseconds, as demonstrated in studies where intracellular recordings were performed in human subjects by Ludin [24]. Figure 3.3 shows a representation of the IAP that includes the slow repolarization phase.
This IAP model was considered in [25]. In that paper, McGill and Lateva showed that it would be possibile to divide a CMAP into a component related to the IAP spike and one related to the negative afterpotential. This division could be possible by estimating the IAP parameters from a CMAP, using a sophisticated mathematical model. However, since the pathological CMAPs at our disposal have shapes far from the ideality due to the abnormal temporal dispersion, that model inversion to separate the two contributions was not a solution applicable in the problem at hand.
The MUAP shape (and by extension the CMAP shape) depends on two main factors:

1. motor unit characteristics (conduction velocity, architecture)

2. muscle-fiber membrane (IAP parameters)

At recording sites close to the fibers, the shape of the IAP has a strong influence on the shape of the MUAP. At more distant sites, however, such as surface recording sites, the MUAP shape depends more on the anatomy of the muscle and the characteristics of the volume conductor than on the shape of the IAP. Nevertheless, the IAP negative afterpotential is a feature that does have a strong effect on the MUAP shape, even at distant recording sites, as demonstrated by several simulation studies ([26],[27]) .

The extracellular potential can be seen as the convolution between a source function related to the IAP and a weighting function related to the muscle unit characteristics.

When the slow repolarization phase is included in the IAP model like in Figure 3.3, the simulations produced CMAPs with higher similarity with experimental signals than the case in which no negative afterpotential is considered in the IAP [23].

From a practical point of view, we need to find a way of modelling the slow repolarization phase of the IAP on the CMAP. It is not a simple task and should be addressed with the main goal of producing a good initial estimation of the kernel. After the terminal standing wave , the CMAP shape is determined exclusively by the slow repolarization of the muscle fibers. This contribution is modelled by an exponential whose time constant is estimated as in Figure 3.4. The time constant determination procedure will be detailed in section 3.4 and represent the first, fundamental step to estimate the kernel. Note that the exponential is only the first

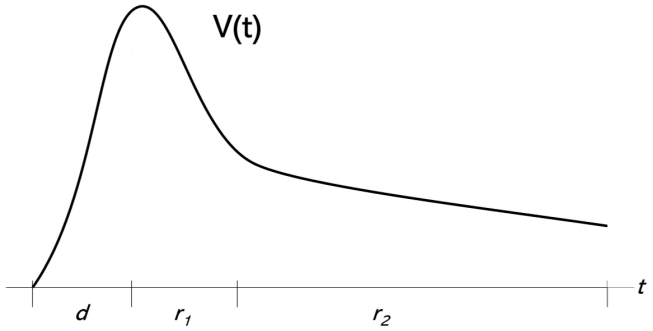

Figure 3.3: Model of IAP including the negative afterpotential. The IAP $V(t)$ consists of a depolarization stage with duration of about 1.5ms (d), a rapid repolarization stage (r_1), and a slow repolarization stage(r_2). The slow repolarization or negative afterpotential can be modelled as a descending exponential with duration of tens of milliseconds.

step to model the slow afterwave contribution on a CMAP, as a sigmoid function was used to smooth its contribution on the biphasic section of the CMAP.

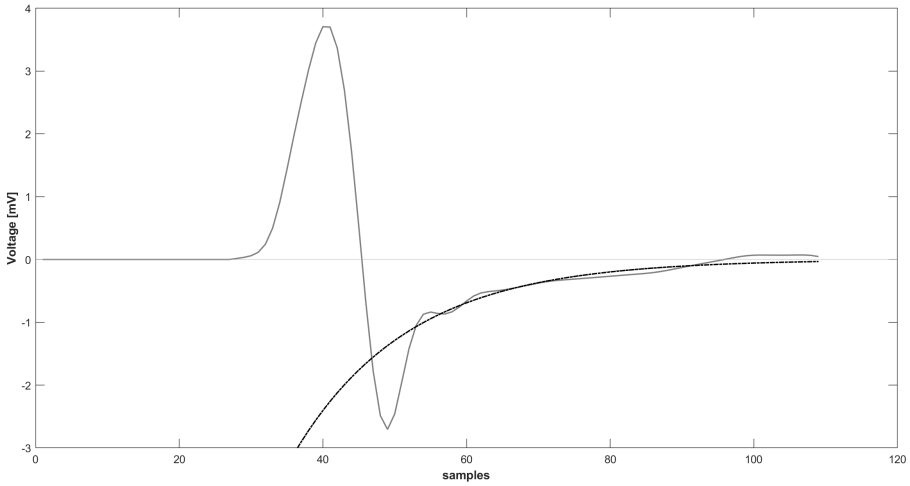

Figure 3.4: Example of exponential fitting and time constant τ estimation. Thenar CMAP (solid line) and the fitted exponential (dotted line). The slow return to baseline of the CMAP is modelled to be included in the kernel.

We can now conclude this discussion about the slow afterwave in muscle potentials by pointing out some important features and characteristics that may be helpful in future studies and application in which the slow return to the baseline needs to be taken in consideration.
First of all, the majority of signals at hand were filtered in the frequency band 5 Hz – 10 KHz and a small number in the band 2 Hz – 10 KHz. The high-pass filter setting of 5 Hz is a conventional value and allows the recording of important low-frequency component of the EMG signal like the slow afterwave. With higher high-pass filter cut-off frequency values (e.g., 20Hz), the slow afterwave may appear distorted and also other important components of the EMG signal may be filtered out. Lateva and Mcgill demonstrated that the slow afterwave is not a filtering artifact but it is instead an actual component of the recorded signal. In addition, they attested that the slow afterwave amplitude is inversely proportional with the temperature. This relation is justified by several studies of the IAP at intracellular level. In our signals, the temperature was not controlled so this test could not be repeated. However, Dr.Cocito and his equipe referred that usually the hand muscle temperature during NCS is around 35°C.

The IAP negative afterpotential is representative of the muscle membrane excitability and increases with peripheral fatigue and intracellular calcium concentration (which may be abnormally elevated in some myopatic conditions)[28].

Further experimental studies based on the analysis of the belly/tendon CMAPs terminal phase would allow to distinguish between the effects of the negative afterpotential and the higher desynchronization in muscle fiber activation.

To sum up, the slow afterwave (SAW) should be considered as an actual component of the CMAP as it emerges from the electrical activity produced by muscle contraction. This assumption was the result of a long and complex analysis and was considered viable on the basis of the literature most established papers regarding MUAP and CMAP electrogenesis. The modelling and inclusion of this component in the kernel was the turning point for tuning the deconvolution method for CB estimation on pathological subjects.

3.3 Deconvolution

In this section it is assumed that the kernel shape is known (the kernel estimation is described in detail in 3.4). In this situation, estimating the delay distribution requires to invert the convolution operator, performing deconvolution. This problem solution is the delay distribution $x(t)$ from equation (3.4), whose integral reflects the number of active MUs and is used to estimate CB.
As previously introduced, solving this problem is difficult as it requires to go in the

opposite direction with respect to causality, making it an inverse problem. In this kind of problems many different causes may produce similar effects. This concept, in the problem at hand, refers to phase cancellations between different sources which may cancel out their effect resulting in similar recorded CMAPs. In addition, the solution of an inverse problem is usually very sensitive to noise and to the approximations introduced in the model (3.2).

The linear system (3.4) solution present some issues: the kernel matrix $\underline{K}$ is not invertible since it is rectangular (see 3.6) and the noise oscillations contained in $n(t)$ cannot be represented by the kernel.

Because of these issues, the deconvolution problem must be solved in the least mean square sense, which corresponds to solve an optimization problem aiming to fit the experimental data ($v(t)$) and the CMAP model ($K(t) * x(t)$), by minimizing the squared error:

$$\min \|v(t) - K(t) * x(t)\|^2 \tag{3.5}$$

Solving this problem numerically requires the discrete versione of each element since our data is sampled in time. Considering M samples, the kernel is a $M \times M$ diagonal-constant matrix, which discretize the convolution operator by including delayed versions of the kernel

$$\underline{K} = \begin{bmatrix} k_1 & 0 & \dots & 0 \\ k_2 & k_1 & \ddots & \vdots \\ \vdots & \vdots & \ddots & 0 \\ k_M & \dots & k_2 & k_1 \end{bmatrix} \tag{3.6}$$

where k_i, $i = 1, \dots, M$, indicates the i^{th} sample of the kernel. Also the CMAP $v(t)$ is sampled, represented by a vector $\vec{V}$ with M samples. The analytical solution of 3.5 is obtained by pseudo-inversion:

$$\hat{x} = (\underline{K}^T \underline{K})^{-1} \underline{K}^T \vec{V} \tag{3.7}$$

where $(\underline{K}^T \underline{K})^{-1} \underline{K}$ is the pseudoinverse matrix of $\underline{K}$. It is equal to the inverse of $\underline{K}$ if the matrix is invertible and it generalizes the inversion in the cases in which $\underline{K}$ is rectangular, like in this problem. This type of solution presents large oscillations reflecting phase cancellations, due to the instability of the problem (see Figure 3.5).

Our goal was to decode the determinism included in the data, represented by the MUAPs composing the CMAP, avoiding to fit the noise. Thus, to avoid the possibility that many sources were included to fit details in the data (producing mostly phase cancellations), some a-priori informations were introduced in the solution. The regularization methods are used to find the correct balancing of fitting data and following a-priori informations. In this work, Tykhonov regularization was

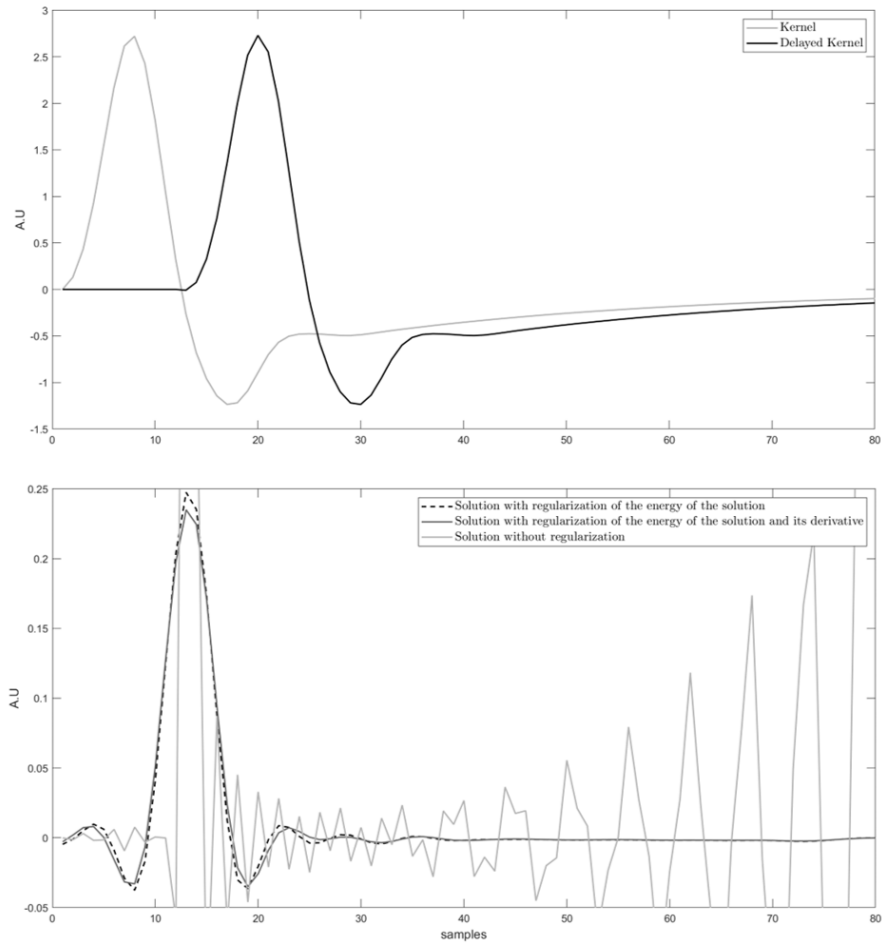

Figure 3.5: Application of the Tykhonov regularization method .**Top** Example of simple simulation, in which the kernel is exclusively delayed. **Bottom** Estimation of the delay distribution using deconvolution. Large oscillations characterize the solution when no regularization method is applied. The oscillations are removed when contraints about the solution are imposed with Tykhonov regularization method.

considered to stabilize deconvolution [29]. Using this method a-priori informations were introduced by adding constraints to the functional to be minimized. In particular, the solution norm (or regularization term) was included, in addition to the residual norm (i.e., the mean squared error in fitting data)

$$\underbrace{\|v(t) - K(t) * x(t)\|^2}_{\text{residual norm}} + \underbrace{\gamma \|x(t)\|^2}_{\text{solution norm}} \tag{3.8}$$

The solution norm depends on the delay distribution and it was used to impose the constraints to the solution. In our case, the solution norm depends on the energy of the solution and the energy of its derivative so that minimizing this functional allowed to obtain a smooth solution with small energy. In particular, the delay distribution smoothness was obtained by minimizing the energy of its derivative. As a result, the regularization problem is:

$$\min \|v(t) - K(t) * x(t)\|^2 + \|x(t)\|^2 \tag{3.9}$$

where

$$\|x(t)\|^2 = \alpha \|x(t)\|^2 + \beta \| \frac{dx(t)}{dt} \|^2 \tag{3.10}$$

Note that since there are two terms to take into account, the penalization parameter γ is splitted into two coefficients that weight their respective terms, α and β. Thus, the solution of 3.9 depends on the penalization parameters α and β. Their values should be chosen in order to obtain a compromise between data fitting and the solution regularization.
The numerical solution of the regularized problem 3.9 is

$$\hat{x} = [\underline{K}^T \underline{K} + \alpha \underline{I} + \beta \underline{F}^T \underline{F}]^{-1} \underline{K}^T \vec{V} \tag{3.11}$$

where $\underline{F}$ is the discretized first derivative operator, with size $(M-1) \times M$

$$\underline{F} = \begin{bmatrix} -1 & 1 & \dots & \dots & 0 \\ 0 & -1 & 1 & \ddots & \vdots \\ \vdots & \ddots & \ddots & \ddots & \vdots \\ 0 & \dots & 0 & -1 & 1 \end{bmatrix} \tag{3.12}$$

Note that the solution $\hat{x}$ in 3.11 requires the inversion of the matrix $M = [\underline{K}^T \underline{K} + \alpha \underline{I} + \beta \underline{F}^T \underline{F}]$. This operation can be source of high errors if the matrix is ill-conditioned , which means that to a small perturbation in the data may correspond an high error in the solution. This concept is related to that matrix condition number k (ratio between maximum and minimum eigenvalue). In particular,

with high k values (usually for $k > 10^3$), the inverse problem will typically be ill-conditioned . That is the case of the matrix $\underline{K}^T\underline{K}$ present in the un-constrained solution 3.7, which has in general high condition number, proof of the original, unconstrained problem instability. In other terms, the original problem cannot be solved without regularization as the error in fitting data is extremely susceptible to litte data perturbations (i.e., noise).
The regularized problem adds some important information about the solution but its solution needs to be stable with respect to both noise and approximations. Both α and β values were chosen to ensure this. In our case, good performance of the regularization method was obtained simply fixing $\alpha, \beta = 10^{-2} \cdot \lambda_{max}(\underline{K}^T\underline{K})$, where $\lambda_{max}(\underline{K}^T\underline{K})$ is the maximum eigenvalue of the matrix $\underline{K}^T\underline{K}$. With these value of α and β, the maximum condition number k of the matrix to be inverted in 3.11 is 100, proving that the inverse problem has become well-conditioned.

Landweber method

Further to the above described constraints related to a-priori informations of the solution, physiological constraints are imposed.
First of all, the solution $x(t)$ must be non negative. In fact, the value assumed by $x(t)$ at a specific time delay $t = \tau$ stands for the number of MUAP recorded at that time by the belly electrode. A negative value of such quantity as no physical meaning.
In addition, the time delays distribution support is bounded to an interval corresponding to the physiological range of CVN.
The boundaries of the CVN range ($CVN_{\min}$ and $CVN_{\max}$) are chosen on the basis of the specific stimulated nerve. The physiologic CVN range of the stimulated nerve should be known and used as a reference. Moreover, the range of conduction velocities in a peripheral nerve is extremely altered when it is affected by pathologies that attack the myelin sheat or others functional elements to the nerve conduction. In particular, the lower bound of the CVN distribution can be extremely lowered with respect to the healthy physiological value. For this reason, the $CVN_{\min}$ value must be chosen with higher attention, considering the higher variance with respect to $CVN_{\max}$ which can usually be chosen equal to the healthy nerve value. See Figure 3.6 for an applicative example.

A projected Landweber method was used to impose the physiological constraints above described. The Landweber algorithm was first introduced in the 1950s and since then it has been applied to solve ill-posed linear inverse problems. Its usage has been extended to non-linear problems that involve constraints.
The Tykhonov solution x_0 is iteratively updated in the direction of steepest descent of the square error functional $\|\underline{K}\hat{x} - \vec{V}\|^2$ and then projected onto the constrained

set:

$$\begin{cases} x_k = x_0 & \text{with } k = 0 \quad (3.13a) \\ x_{k+1} = \max(y_{k+1},0) & x_{k+1}(\bar{S}) = 0 \quad (3.13b) \\ \mu = \dfrac{0.9}{\lambda_{max}(\underline{K}^T \underline{K})} & (3.13c) \\ y_{k+1} = x_k - \mu \underline{K}^T(\underline{K} x_k - \vec{V}) & (3.13d) \end{cases}$$

where k is the iteration, $\mu \underline{K}^T(\underline{K} x_k - \vec{V})$ is the solution updating rule, μ is the step size parameter and $\bar{S}$ is the complement to the constrained support of the solution. The μ value is chosen to obtain the algorithm convergence in about 10 steps. To obtain the time delays boundaries that bound the solution support $\left[\frac{d}{CVN_{\max}}, \frac{d}{CVN_{\min x}}\right]$, the distance from the stimulation site to the motor point must be measured during the NCS. If the stimulation distances are not reported, they could be estimated on the basis of the conduction velocity.

3.4 Estimation of the Kernel

The solution of 3.9 requires the estimation of the kernel $K(t)$. Tu et al., 1997, proposed a kernel model aiming to estimate the distribution of conduction velocity of peripheral nerve fibers. That model was based upon two assumptions: 1) constant CVN along the stimulated nerve, 2) CB absence. A further approximation was that of using the relation between conduction velocity and MUAP amplitude to determine the kernel shape. In our case, the time delay distributions depends on the time delay due to nerve conduction and due to muscle fiber conduction, as described in section 3.1. Furthermore, the CMAPs of interest in the problem at hand are the result of a subtotal MUAP summation, due to CB presence. Finally, the relation between CVN and MUAP amplitude is not precise, since the MUAP amplitude recorded on the skin depends on the MU location, and thus it was not used in this work.
For all this reasons, a new kernel model was developed and optimized for the pathological subjects.

The kernel was estimated by an optimization method with the goal of minimize the mean square error in reconstructing both $v^{dist}(t)$ (CMAP obtained with distal stimulation) and v^{prox} (CMAP obtained with proximal stimulation), defined as :

$$MSE[K] = \left\| v^{dist}(t) - K(t) * x^{dist}(t) \right\|^2 + \left\| v^{prox}(t) - K(t) * x^{prox}(t) \right\|^2 \quad (3.14)$$

where $x^{dist}(t)$ and x^{prox} are the time delay distributions related to distal and proximal CMAP, respectively.

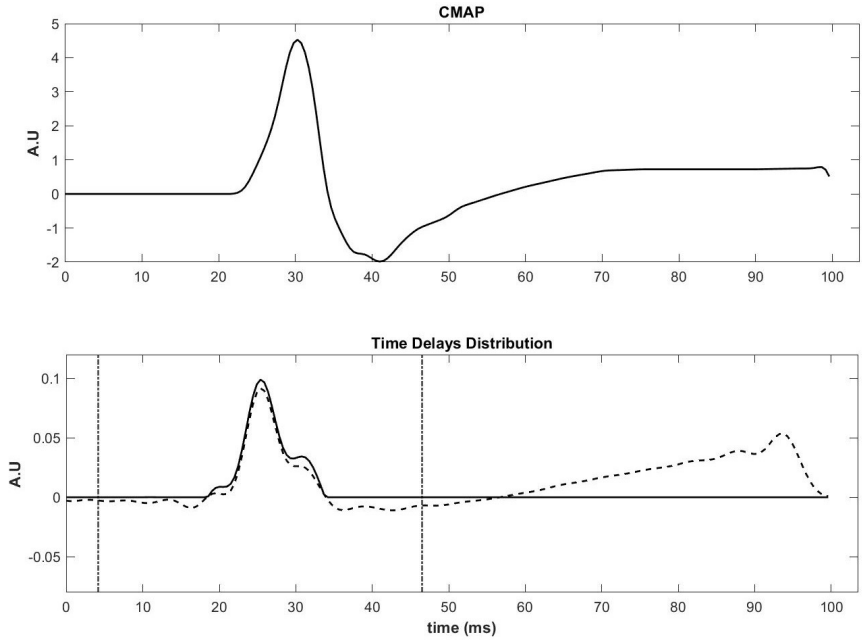

Figure 3.6: Example of Landweber method application. **Top**: CMAP in which the tail crosses the baseline. **Bottom**: Estimated time delay distribution.The deconvolution method elaborate this portion as informative and the estimated delay distribution assumes positive values in its corrispondence (after 60 ms). However, this delay distribution section is not related to MUs activity. For this reason, the mentioned section of the distribution is removed by applying physiological limits with the Landweber method (stretch point line). Negative values of distribution and values outside the constrained support are imposed to be zero (solid line).

The kernel is a representative MUAP that, when convolved with $x^{dist}(t)$ and x^{prox}, produces an approximated reconstruction of the recorded CMAPs. The kernel shape was computed blindly, meaning that we just assumed it to be consistent with a MUAP extracted from a CMAP acquired by a belly/tendon montage. The reference on which the initial kernel shape was determined is the distal CMAP. This is simply because the temporal dispersion is proportional to the conduction distance, hence it is slower in the distal CMAP and thus the waveform is less dispersed in time and viable for shape reconstruction.

On the basis of [30], a MUAP can be well represented by the Associated Hermite (AH) functions. The AH functions are obtained multiplying the Hermite polynomials with appropriate Gaussian functions (see equation 3.16) and are also referred to as *wavelets*. These functions are more suitable to describe the MUAP shape (and in general the shape of compact support signals) with respect to Fourier

analysis since they have compact support and their parameters can be flexibly set in order to reproduce the signal shape.

According to [19], we decided to express the kernel as the linear combination of the first six AH functions since using more functions only increased the computational time while leaving unchanged the reconstruction performances:

$$K(t) \cong \sum_{n=0}^{5} \beta_{\lambda,n} \mu_{\lambda,n}(t) \tag{3.15}$$

where

$$\mu_{\lambda,n}(t) = \frac{1}{\sqrt{2^n n!}} H_n\left(\frac{t}{\lambda}\right) \frac{1}{\sqrt{\sqrt{\pi}\lambda}} e^{-\frac{t^2}{2\lambda^2}} \tag{3.16}$$

is the set of n Associate Hermite function and H_n are the Hermite polynomials recursively defined as

$$\begin{cases} H_0(t) = 1 \\ H_1(t) = 2t \\ H_n(t) = 2tH_{n-1}(t) - 2(n-1)H_{n-2}(t). \end{cases} \tag{3.17}$$

However, the Associate Hermite functions are not sufficient for the kernel estimation when the CMAP have a tail component (i.e., slow afterwave) with which returns to the baseline.
Figure 3.7 shows the decrease in the reconstruction quality of a CMAP that returns to the baseline without a distinct endpoint using exclusively the AH functions, represented by an altered kernel shape.
The slow afterwave was present in almost every distal CMAP we had at disposal. For this reason, further steps were implemented in order to obtain a good initial estimation of the kernel, which also included the slow afterwave.

As Figure 3.7 shows, the biphasic shape of a CMAP can be well approximated using the Hermite expansion. We can think of an experimental CMAP as if its biphasic portion is summed to a function that represents the slow repolarization of the muscle fibers contribution on the recorded potential. With this mindset (based again on the simulations of Lateva and Mcgill, [25]) , we decided to model this function $f(t)$ using a descending exponential $e(t)$ (fitted over the slow afterwave of the CMAP) multyplied with a sigmoid function $s(t)$ and to include it in the kernel shape. The sigmoid function was introduced for two main reasons: to reduce the exponential contribution over the "biphasic" portion of the CMAP since during the initial standing wave and the termination wave, the effect of the slow repolarization of the muscle fibers has extremely low impact on the CMAP field. Second, we wanted to obtain an initial kernel without dealing with discontinuity points between the biphasic portion of the CMAP and the slow afterwave.

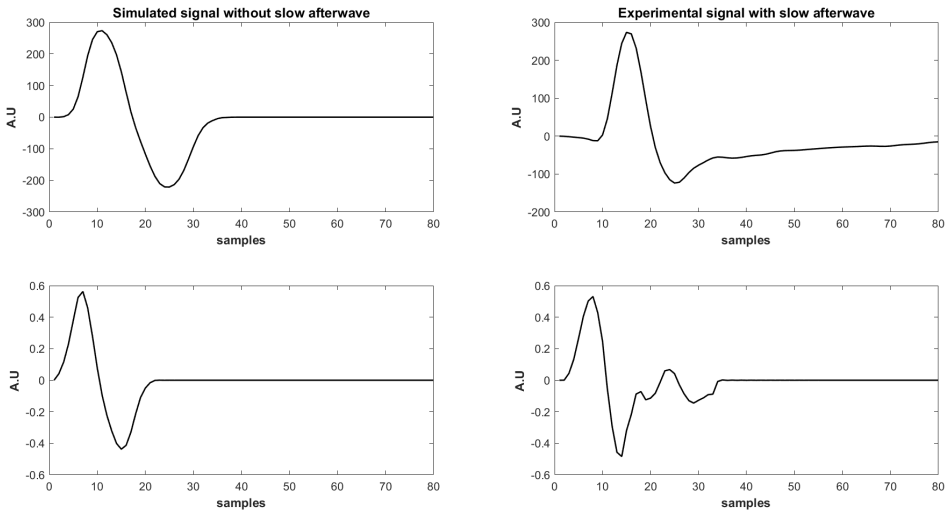

Figure 3.7: Kernel estimation with Associate Hermite functions. **Top row**, distal CMAPs used to obtain the initial kernel. *left*: simulated CMAP without slow afterwave, *right*: experimental CMAP with slow afterwave. **Bottom row**: initial kernel estimation using the AH functions. *left* : the AH functions approximate well the biphasic shape of the simulated CMAP, *right*: the AH functions fail to reconstruct the slow exponential component and the kernel shape is altered.

Figure 3.8 shows the function $f(t)$ determination for a practical case in which the slow afterwave is present.

The function $e(t)$ has two parameters that are chosen to optimally fit the CMAP section defined starting from an automatically detected inflection point. The inflection point was determined as the first point where the mean and the slope of the signal changed most abruptly after the absolute minimum. The starting point of the optimal CMAP section for the exponential fitting was then defined using an interval of 5 ms centered on this point while the endpoint was always the last point of the CMAP.
The sigmoid function $s(t)$ has two parameters, which optimal values were chosen by minimizing an objective function consisting of two terms:

- difference between the intermediate CMAP $v_1(t)$ and the corrispective kernel obtained with AH functions exclusively $K_{AH}(t)$
- difference between the first phase of the original CMAP $v(t)$ and the intermediate CMAP $v_1(t)$

With this procedure, the Associate Hermite functions could estimate successfully a biphasic kernel starting from a CMAP with the slow afterwave indicated with

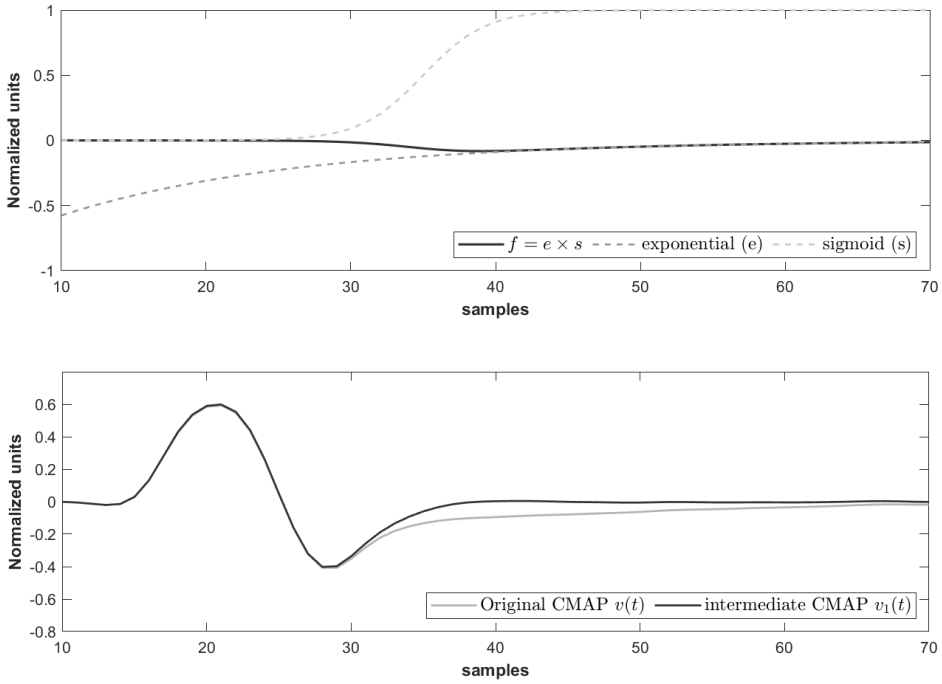

Figure 3.8: Estimation of the slow afterwave from an experimental CMAP. **Top**: The slow repolarization contribution is modelled by the function f as the multiplication of an exponential e and a sigmoid s whose parameters are optimized for each specific CMAP. **Bottom**: The function f is subtracted from the experimental CMAP $v(t)$ obtaining an intermediate CMAP shape $v_1(t)$ for which the kernel estimated with AH function exclusively (termed $K_{AH}(t)$) is optimal.

$K_{AH}(t)$ in Figure 3.9.
Once $K_{AH}(t)$ is obtained, it is summated with $f(t)$. As a result, the initial estimation of the Kernel $K_0(t)$ is obtained.
Notably, this refined procedure of initial kernel estimation led to a substantial increase in the deconvolution method performances mostly in cases where the CB estimation was performed over abnormally dispersed CMAPs that also presented the slow afterwave.

The initial estimation of the kernel is determined solely using the distal CMAP. However, the deconvolution method requires that, by using the same kernel, both CMAPs could be well reconstructed using the two estimated time delay distributions. In order to fullfill this requirement, the optimal kernel shape was determined by an iterative optimization method based on the gradient of the reconstruction error E,

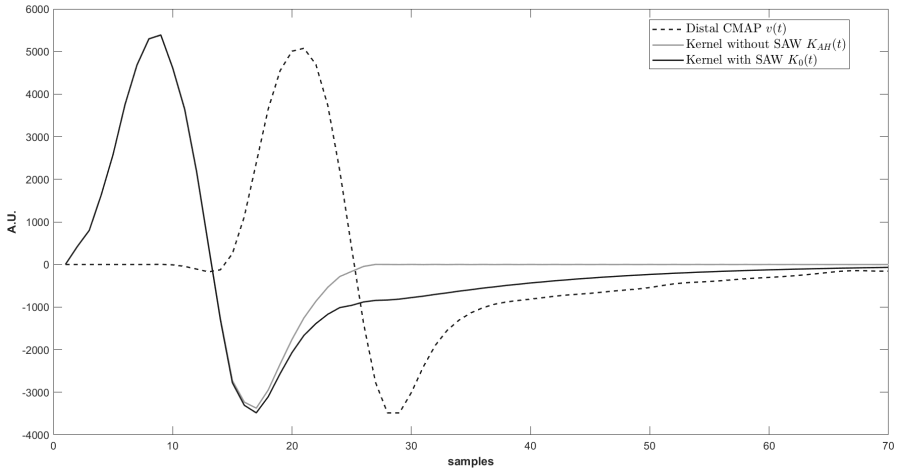

Figure 3.9: Estimation of the initial Kernel from distal CMAP. The slow return to baseline is correctly modelled in the initial kernel $K_0(t)$ (black line) with the described procedure.

defined as:

$$E = \frac{\sqrt{MSE[K]}}{\sqrt{\|v^{dist}(t)\|^2 + \|v^{prox}(t)\|^2}} < 8\% \tag{3.18}$$

which includes both CMAPs' reconstruction error.
The optimization method was initialized with $K_0(t)$ and updated the parameters vector $\vec{p}$ defining the kernel in the direction opposite to that of the gradient of MSE. The updating rule was the following:

$$\vec{p_i} = \vec{p_i} - \mu \frac{\nabla MSE}{\|\nabla MSE\|} \tag{3.19}$$

Where the parameters vector $\vec{p}$ consists of:

- seven parameters related the AH functions: the scaling factor λ and six coefficients $\beta_{\lambda,n}$ (see Eq. 3.15).
- two parameters defining the descending exponential $e(t)$, namely the amplitude A and the time constant τ : $e(t) = Ae^{-\frac{t}{\tau}}$.
- two parameters defining the sigmoid function $s(t)$, namely the time istant c in which $s(t) = 0.5$ and the rate of change a : $s(t) = \frac{1}{1+exp^{-a(t-c)}}$.

for a total of eleven parameters that were iteratively updated to obtain the lower E possible.

The step parameter μ choice was made in order to obtain a good compromise between stability and convergence rate. We wanted this trade-off choice to produce a computational time of the iterative method of the order of 1 min and possibly lower while assuring a good convergence rate. In order to do so, the minimum of MSE in the direction of the gradient was computed at each iteration with a four step dicotomic search of the μ value with starting value $\mu = 0.25$. The optimization procedure could be further studied and improved to obtain an automatic step size value for each considered CMAP using more complex algorithms. The updating rule (3.19) was executed until the reconstruction was lower that 8% or for a maximum of ten iterations.

The required precision of 8% is a very strict condition to satisfy. In fact, we can note from Eqs. (3.14) and (3.18) that to $E = 10\%$ corresponds a SNR value of 20dB, which is a very common value in experimental EMG signals acquired over the skin. Hence, in ideal conditions, a 10% reconstruction error of the deconvolution method could be attributed to the various sources of noise that are typically present in experimental signals (e.g., powerline interference).

To improve the reconstruction quality, an additional optimization method was implemented, initialized with the last estimated kernel of the first method. This second method aimed to reduce the reconstruction error below the required 8% by slightly modifying the kernel samples within a support defined as the region where the the kernel amplitude is higher that the 2% of its range. The iterative procedure of this second optimization method is very similar to the first method's one, with the maximum number of iterations set to five and with an initial value of μ equal to 0.125.
This second step has low impact on the kernel shape and thus on the reconstruction error with respect to the first one. The sequence of the two optimization methods is described in the method's block diagram, shown in 3.10.

3.5 Estimation of CB from the delay distributions

The CB estimation is obtained using the integral of both delay distributions which are considered an estimation of the number of active motor units (MUs):

$$CB = 1 - \frac{\int x^{prox}(t)dt}{\int x^{dist}(t)dt} \tag{3.20}$$

We have to note that the number of MUs reflected by the delay distribution integral may be biased by large MUs close to the belly electrode. This is expecially true when the detection volume of the belly/tendon montage cannot cover the entire muscle fibers length (e.g., electrodes positioned over the Tibialis Anterior (TA) after

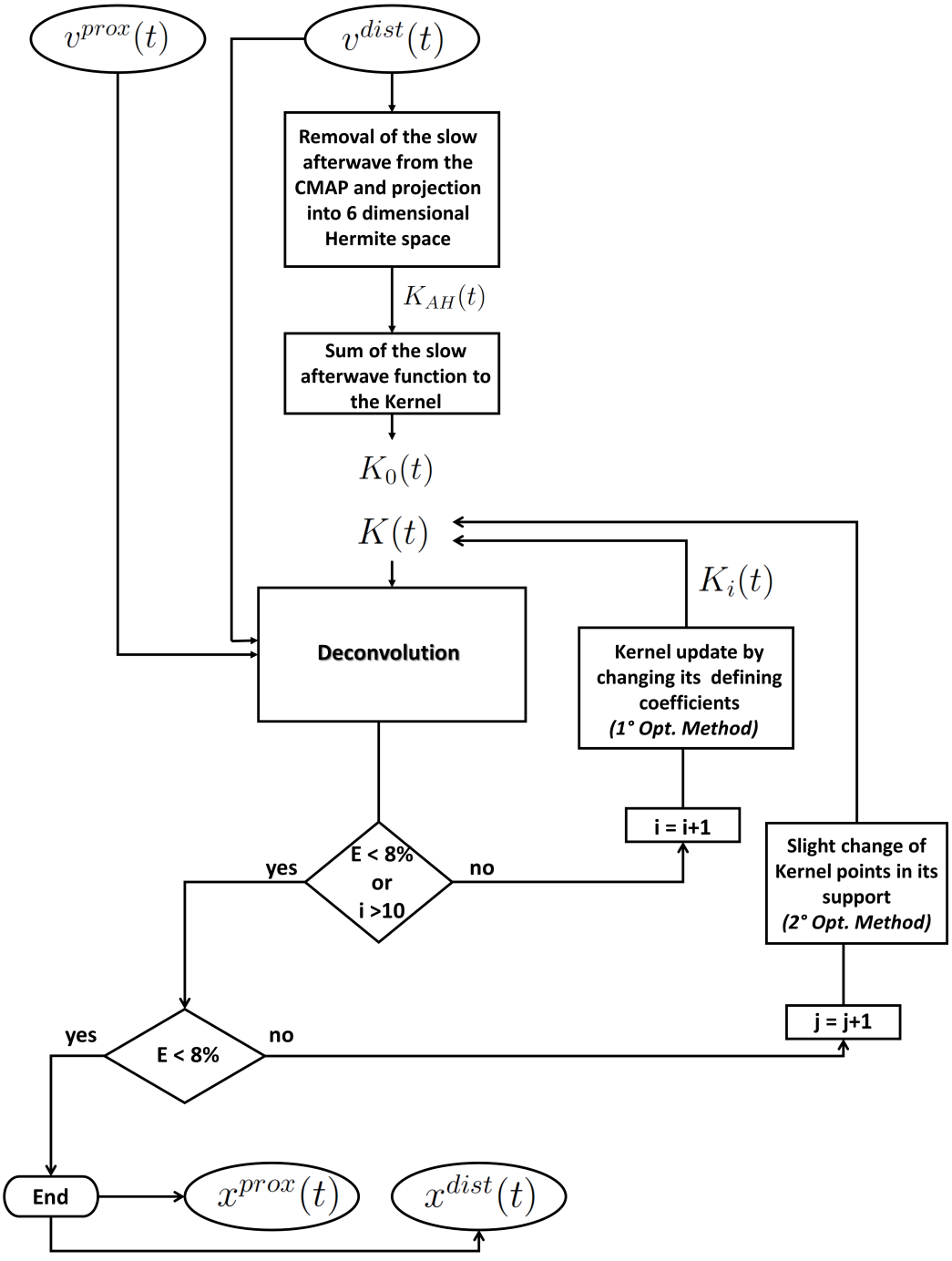

Figure 3.10: Block diagram of the proposed method.

a stimulation of the peroneal nerve). However, the majority of motor NCSs are performed recording EMG signals produced by hand muscles (mostly from thenar and hypothenar eminences) using large electrodes. In these common situations, the detection volume would be sufficient to cover the totality of the muscle activity and thus the recorded potential amplitude would be less dependent on MU locations. Either way, it should be kept in mind that the CB estimation highly depends on the MUs contribution on the detected CMAPs. Thus, it could be possible to under-estimate the CB if the blocked MUs are small or located at large distance from the detection system. For this reason, the CB estimation has an uncertainty of the order of E.

3.6 Experimental signals

The experimental signals used to test the proposed method were divided in two categories :

- signals manually copied from images of clinical records on paper with an apposite MATLAB routine. We can refer to these signals as *manually digitalised (MD)* since several operations were needed to obtain discrete time series from the scanned (or worse photographed) data provided by Dr.Cocito. The process to obtain these signals is described in details in the following.

- originally digital signals since they were extracted directly from the electromyographic machine. We can refer to these signals as *originally digitalised (OD)* since no pre-processing steps were required to obtain their digital version.

The above described division of the experimental signals used in this thesis is simply based on the fact that clinicians usually don't need the digital signals for their purposes. For this reason, during a routine motor NCS, the only saved output is a clinical record of the evoked CMAPs printed on paper. Further, the pathologies causing abnormal temporal dispersion and/or conduction block are extremely rare, resulting in a low number of subjects producing the signals on which we need to test the deconvolution method. Because of this, we used every signal at our disposition to test the proposed CB estimation method. Figure 3.11 shows an example of clinical image on which a pair of CMAPs is reported and needs to be converted into a pair of time discrete time series. It is important to note the presence of several information on the image : the stimulated nerve and the muscle producing the motor responses, the vertical and horizontal division values, the markers positioned on the CMAPs, the bandpass filter settings and the current delivered at each stimulation site. These informations were fundamental in data processing but their precence on the image made an automatic method to digitalise the waveforms unfeasible.

Since a great number of signals at our disposal was given in the form of images, an appropriate manual method to digitalise the CMAPs was developed.

First of all, the image is cropped to have a close up view on the axis on which the CMAPs are plotted. In all the cases, the image is rotated in the xy plane. The image rotation was compensated by estimating an angle between one deflected horizontal line (defined with two manually selected points on the grid) and an horizontal axis. Additional deformations in the image were not taken into consideration.

The isoelectric line was defined using the first marker (CMAP onset). To remove eventual fluctuations of the copied signal before the CMAP onset, each signal's values were forced to be zero until the first marker. Next, the waveforms were copied using a built-in function of MATLAB that allows to manually select points over an image. With this function, the CMAPs were copied starting from the first point after the stimulation artifact, and their pixel values converted into voltages values using the vertical and horizontal division as reference. The obtained sequence of points was then linearly interpolated using 2048Hz as sampling frequency. The sampling frequency value was chosen to be consistent with the originally digitalised signals and to provide sufficiently smooth waveform (and, obviously, to be higher than the Nyquist frequency). Using higher sampling frequencies didn't improve the method performances on the signals, but only increased the computational time. Finally, all the four automatic markers were saved with the CMAPs, as they provide the CMAPs duration values used by clinicians. The criteria used to find the marked points on the CMAP by the EMG machins are unknown and for this reason the last marker was not used to define the CMAP duration. We decided to use a fixed time interval to apply the deconvolution method to the CMAPs, since no distinct endpoint was present due to the slow afterwave. This time interval was 100 ms if possible, 50 ms otherwise.

Figure 3.12 shows the linear interpolation of the manual points selected on a CMAP and the digital signals obtained with the described procedure.

All the manually digitalised signals at hand were related to pathological subjects. However, in some cases, it was impossible to retrieve the diagnosis with certainty. We assumed that those patients suffered of either Chronic inflammatory demyelinating polyneuropathy (CIDP) or multifocal motor polineurophaty (MNM), as indicated by the doctor who performed the clinical exams.

The originally digitalised signals at hand were related to both healthy and pathological subjects. The CMAPs obtained from healthy subjects are the same used in [19] and refer exclusively to ulnar nerve stimulation, the recording was performed on the right abductor digiti minimi muscle. The proximal site of stimulation was above-elbow while the distal site was either below-elbow or at the wrist, following the experimental protocol of [31]. The distance between the two stimulation sites at the elbow was equal to 100 mm. The distances were 78.5 $\pm$ 3.7

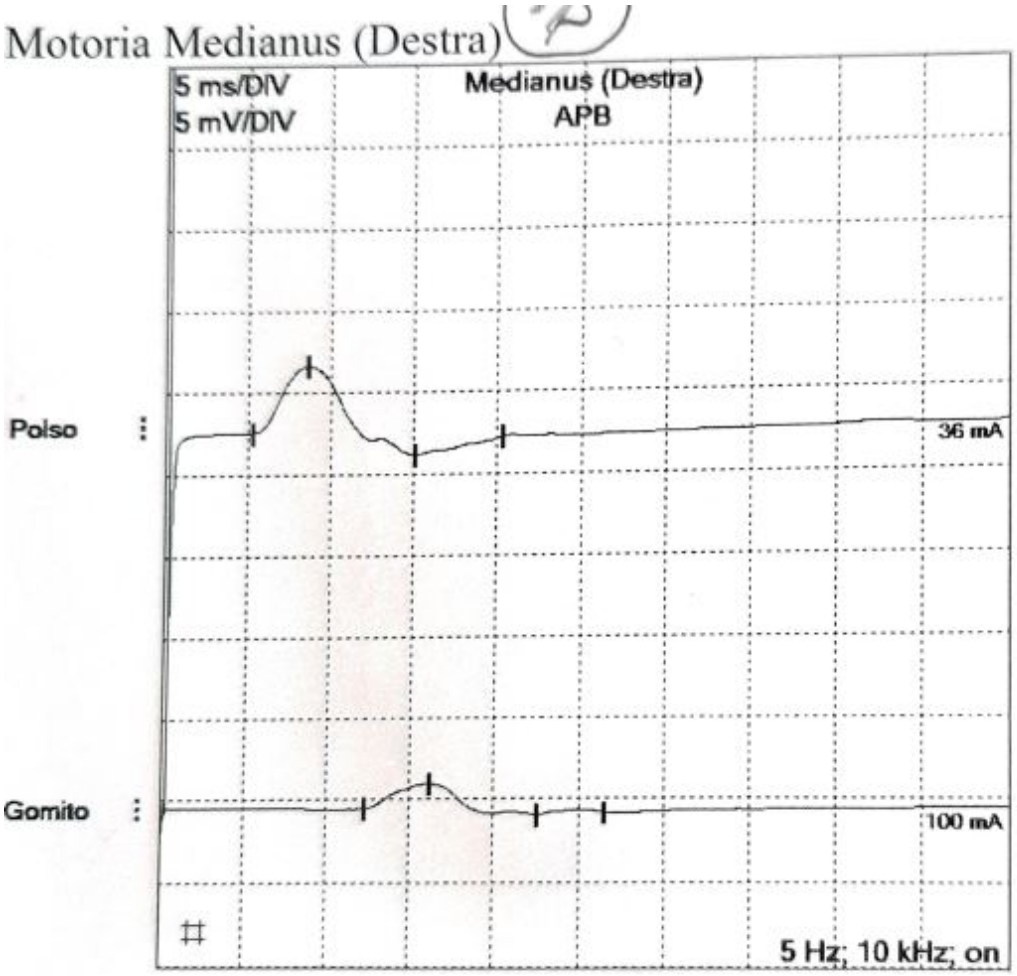

Figure 3.11: Example of motor NCS results on paper. The right medianus nerve is stimulated at the wrist and at the elbow , obtaining a distal and a proximal CMAP, respectively, recorded over the abductor pollicis brevis (APB in the image). Several important informations for data processing like the markers and the bandpass filter cut-off frequencies are obtained from each clinical record.

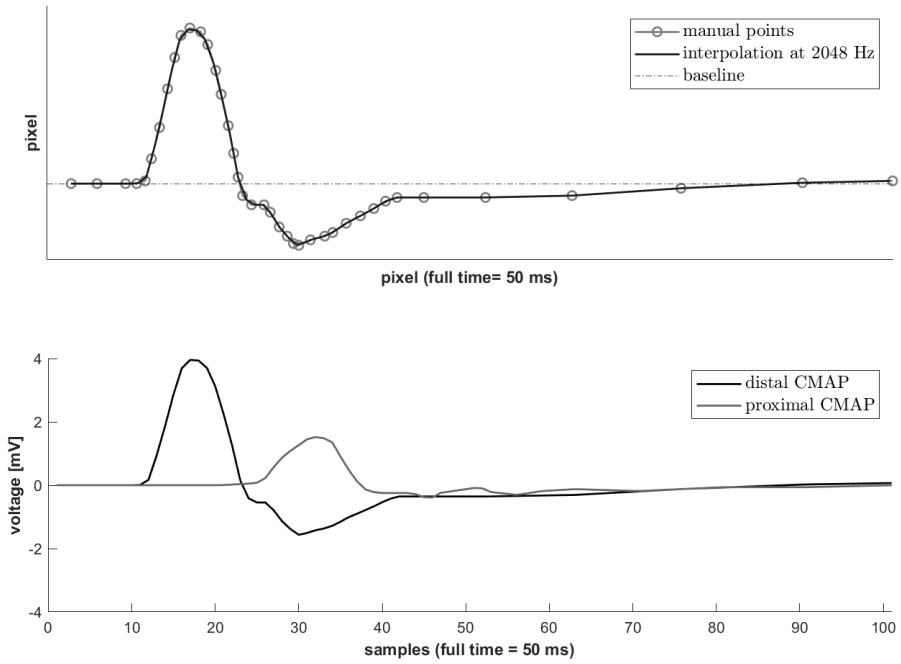

Figure 3.12: Digital CMAPs obtained from low quality images of clinical records on paper. **Top**: Distal CMAP. The waveform points are manually selected and linearly interpolated at 2048Hz. **Bottom**: CMAPs from Figure 3.11, digitalised. The proximal CMAP is dispersed in time and has many oscillations across the baseline of low amplitude. In this case, an higher variability introduced by the manual selection of points is unavoidable.

mm from the motor point to the wrist, 325.4 $\pm$ 18.4 mm from the motor point to below-elbow, 424.2 $\pm$ 17.4 mm from the motor point to above- elbow (mean $\pm$SD). The supra-maximal stimulation was obtained with a 0.1ms long squared bi-phasic pulse and the responses were filtered between 2Hz and 10KHz.
Using the healthy (control) signals, it was possible to test the method performances with two different temporal dispersions by comparing above-elbow with wrist (conduction distance about 350 mm) and above-elbow with below-elbow (conduction distance about 100 mm) and to compare the results with the standard clinical methods.

The main goal of this work, however, was to test the method with pathological signals. The two main pathologies that are involved in the cases in which the abnormal temporal dispersion and the conduction block are present are the CIDP (in which the myelin sheat is attacked by antibodies) and the MNM (in which the

sodium channels are attacked by antibodies). It is mostly in these specific cases that the deconvolution method is expected to outperform standard clinical methods in estimating conduction block.

Chapter 4

Results on experimental signals

4.1 Healthy subjects

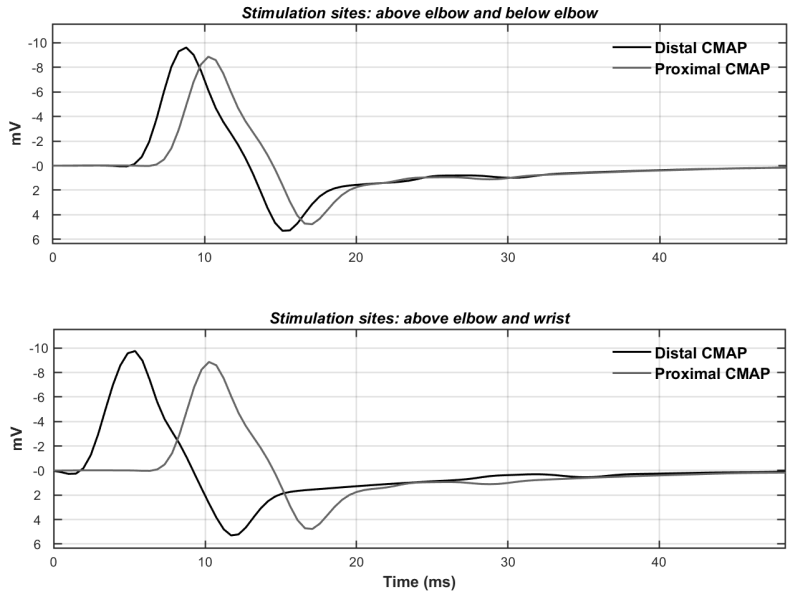

Figure 4.1: CMAPs recorded over the abductor digiti minimi muscle of an healthy subject, elicited by ulnar nerve stimulation. **Top**: stimulation above elbow and below elbow (conduction distance about 100 mm), **Bottom**: stimulation above elbow and at the wrist (conduction distance about 330 mm).

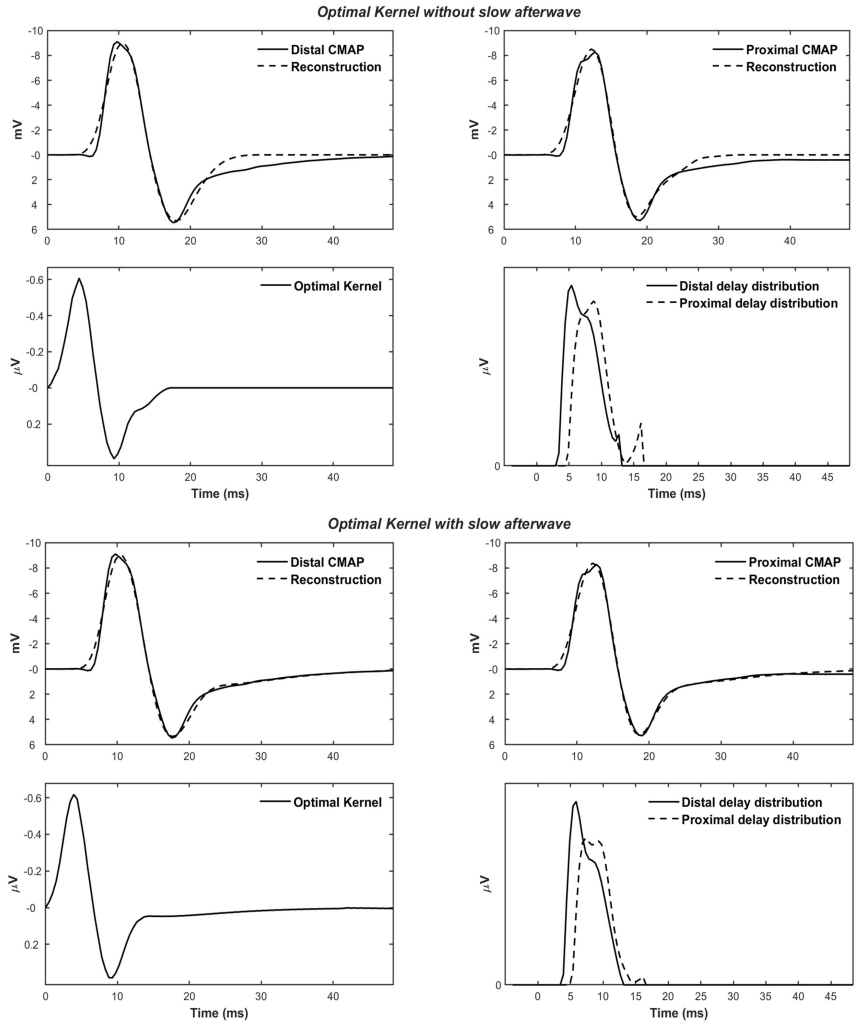

estimated block (amplitude): **9.1 %;**
estimated block (area): **9.6%**
estimated block (deconvolution)**: Kernel without slow afterwave: 8.4%; Kernel with slow afterwave: 8.9%**
Reconstruction error **: Kernel without slow afterwave: 18.6% ; Kernel with slow afterwave: 9.9%**

Figure 4.2: Example of optimal kernel's influence on deconvolution method using experimental signals from an healthy subject. **Top**: the optimal kernel doesn't take into account the slow return to baseline (i.e., the slow afterwave) reflecting high reconstruction error over the terminal portion of CMAPs. **Bottom**: the optimal kernel shape contains an exponential return to baseline, allowing to better reconstruct the terminal portion of both CMAPs.

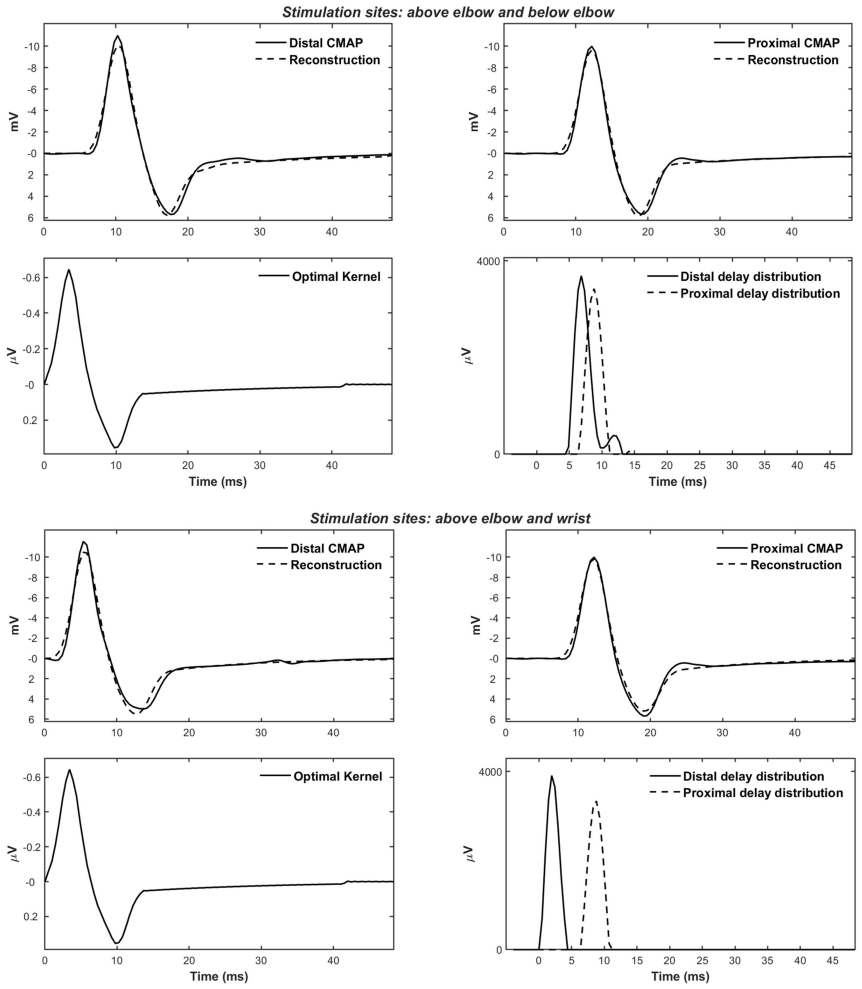

Figure 4.3: Application of deconvolution method to experimental signals from an healthy subject. Different temporal dispersion were obtained by comparing stimulation above-elbow with below elbow (conduction distance about 100 mm) and above elbow with wrist (conduction distance about 370 mm). The distal and proximal CMAP's reconstructions, the optimal estimated kernel and the estimated delay distributions are shown. The CB estimation is compared with the CB estimated with standard clinical methods to assess the impact of different conduction distances.

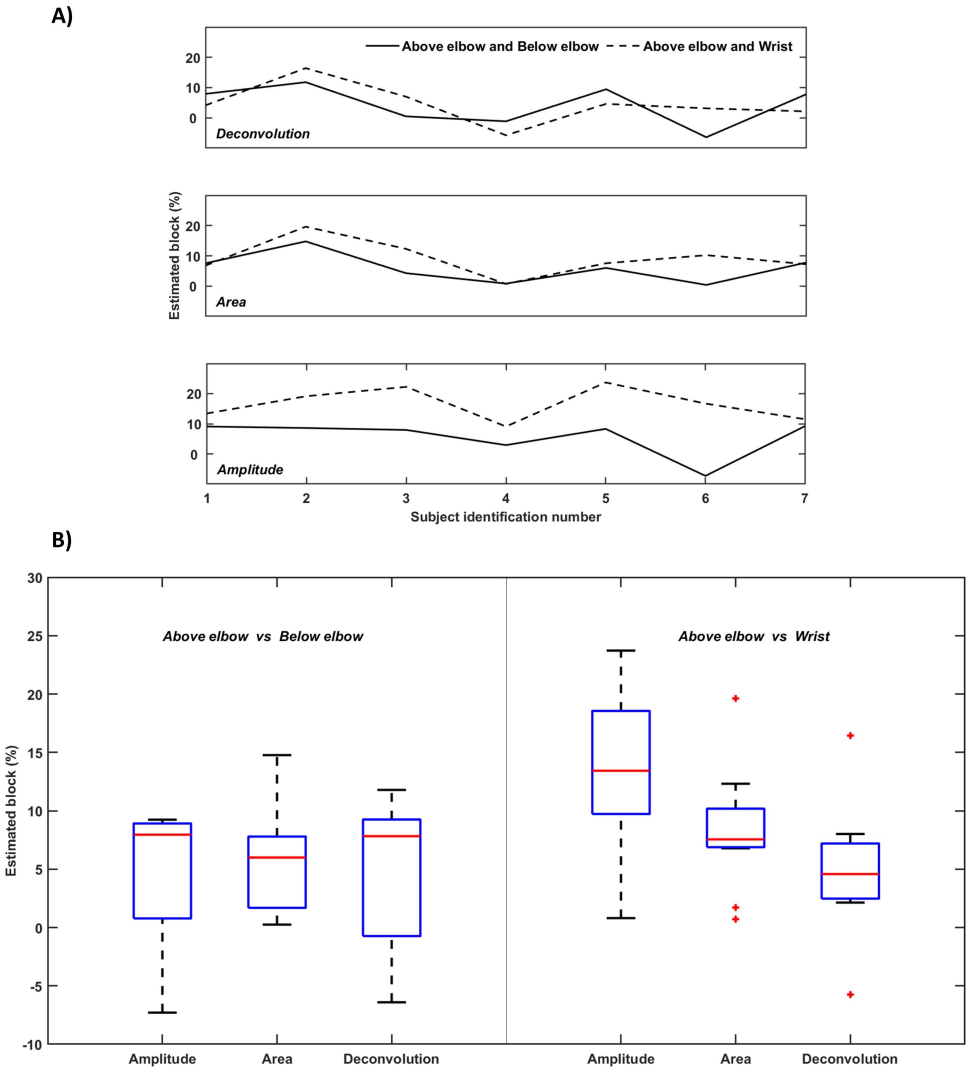

Figure 4.4: Effect of the conduction distance on deconvolution, area and amplitude methods applied to experimental signals from the healthy subjects. **A** Estimated block with the three methods for all considered subjects, considering the two conduction distances separately. **B** Boxplot of such estimates for each method. The red lines are the median values and the red crosses are the outliers, the bottom and top of each box are the 25th and 75th percentiles of the sample, respectively. Both area and amplitude methods are positively biased by temporal dispersion.

4.2 Pathological subjects

4.2.1 Chronic Inflammatory Demyelinating Polyneuropathy (CIDP)

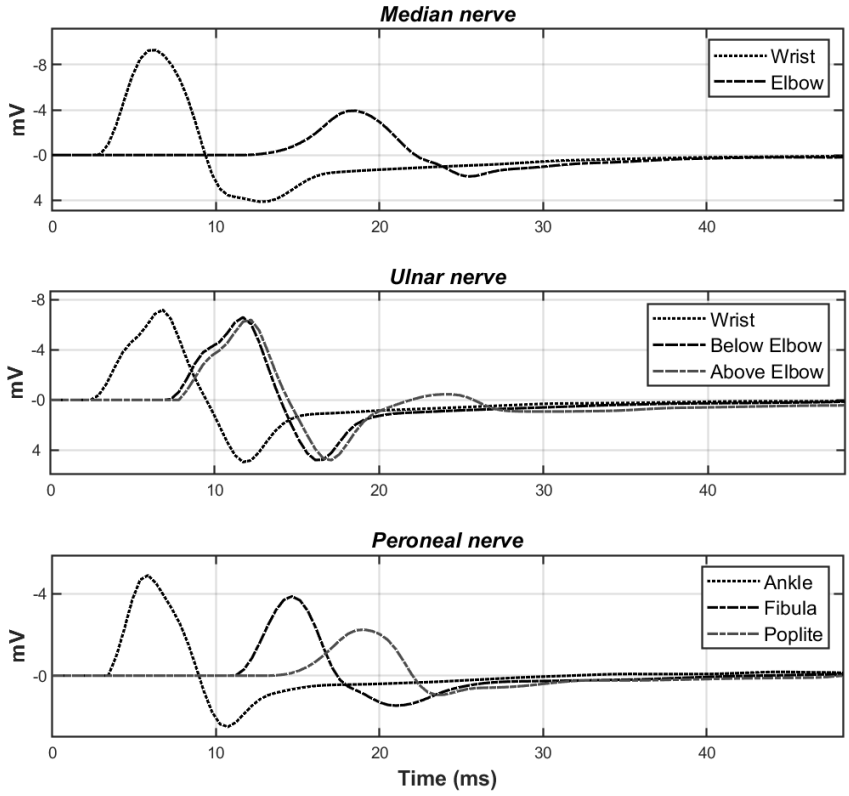

Figure 4.5: Motor responses (CMAPs) of a CIDP patient recorded on *Abp*, *Adm*, *Edb* muscles after median, ulnar, peroneal nerve stimulation, respectively. The reported signals were digitalized with the procedure described in Section 3. For the ulnar and peroneal nerve, two comparisons can be made since the stimulation is performed at three different sites, allowing to study the nerve conduction over segments of different length.

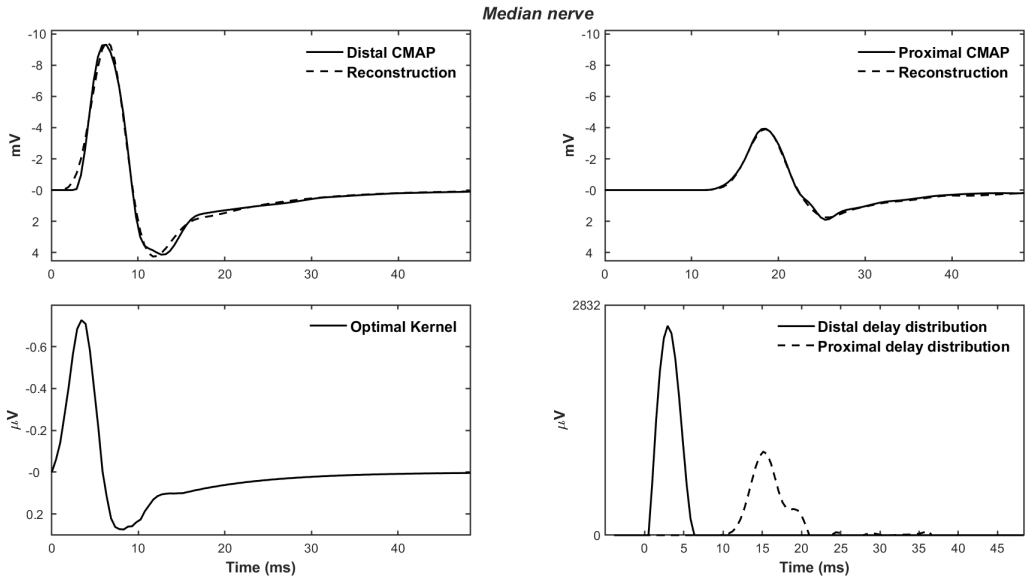

Figure 4.6: Details of CB estimation with deconvolution method using signals elicited by median nerve stimulation of the CIDP patient reported in Figure 4.5. In this case, the CVN value was provided (CVN = 28.4 m/s), so it was possible to estimate the position of both stimulation sites starting from the markers on the clinical records (Figure 3.11). Estimated CB = 41.4 %, Reconstruction error = 8.6 %.

	Conduction block (%)		
Studied nerve	**Amplitude**	**Area**	**Deconvolution**
Median			
wrist, elbow	57.8	47.9	41.3
Ulnar			
wrist, above elbow	11.2	12	7.8
below and above elbow	3.1	4.9	5.6
Peroneal			
ankle, poplite	54.1	38	30.3
fibula, poplite	41.9	25	19.3

Table 4.1: Conduction block estimation results for the CIDP patient signals shown in Figure 4.5.

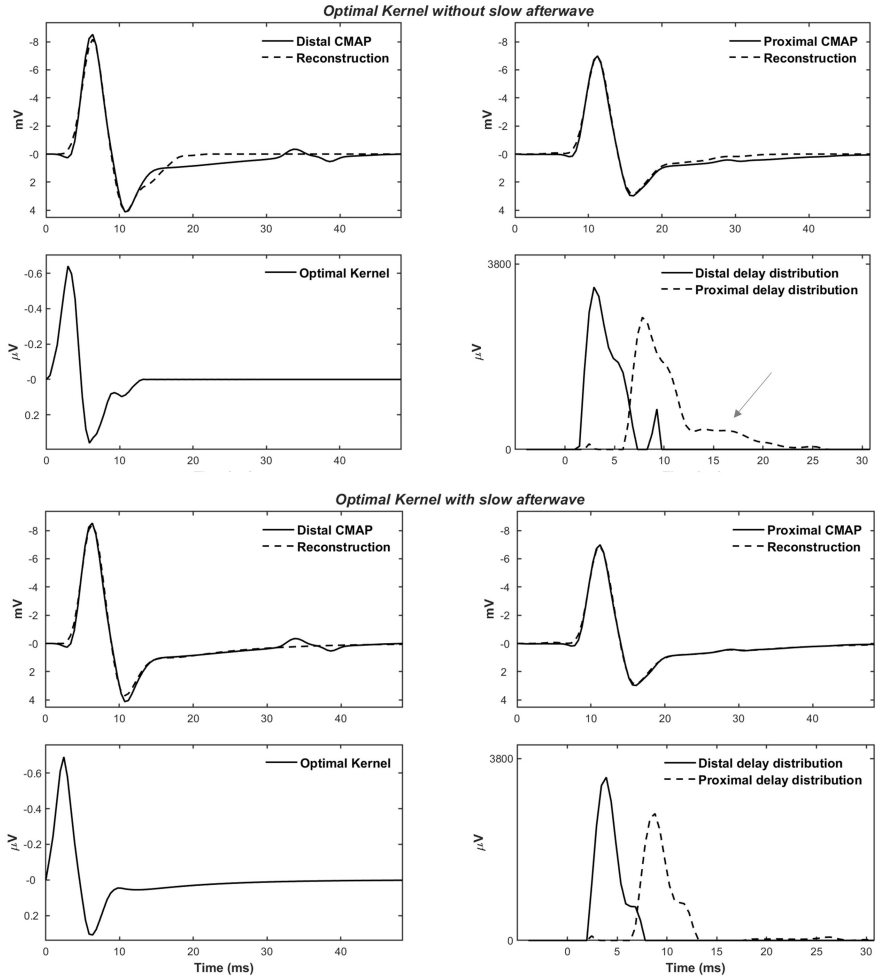

Figure 4.7: Example of optimal kernel's influence on deconvolution method using experimental signals from a CIDP patient. **Top**: the optimal kernel doesn't take into account the slow return to baseline (i.e., the slow afterwave) reflecting high reconstruction error over the terminal portion of CMAPs. **Bottom**: the optimal kernel shape contains an exponential return to baseline, allowing to better reconstruct the terminal portion of both CMAPs. The grey arrow points at the erroneous portion of the proximal delay distribution obtained to reconstruct the slow afterwave of the proximal CMAP. The additional portion of distribution obtained with the kernel without slow afterwave results in a negative estimated CB.

4.2.2 Multifocal Motor Neuropathy (MMN)

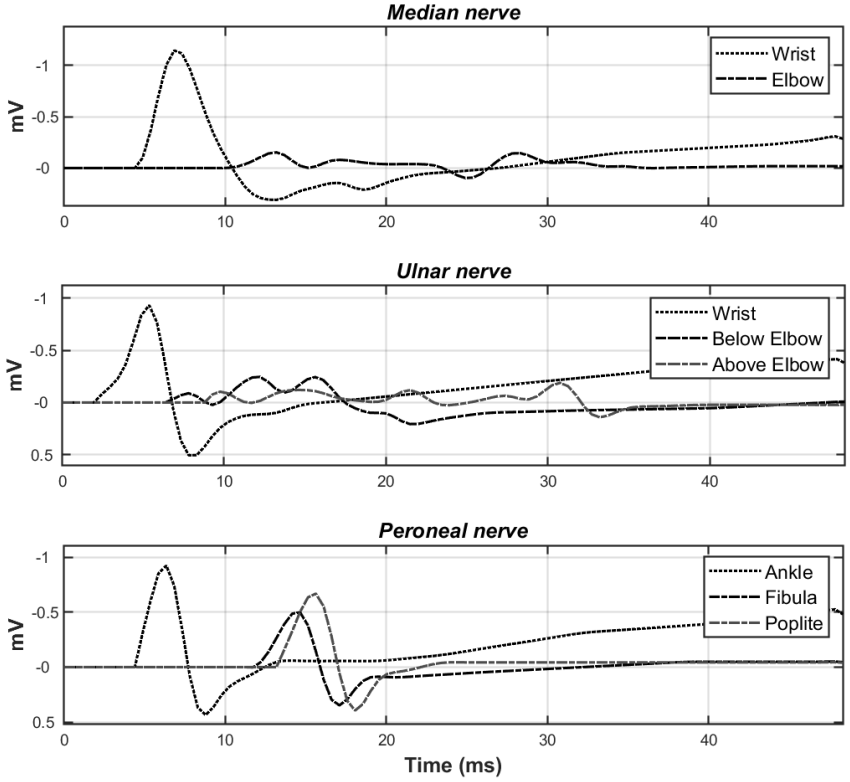

Figure 4.8: Motor responses (CMAPs) of a MNM patient recorded on *Abp*, *Adm*, *Edb* muscles after median, ulnar, peroneal nerve stimulation, respectively. The reported signals were digitalized with the procedure described in Section3. For the ulnar and peroneal nerve, two comparisons can be made since the stimulation is performed at three different sites, allowing to study the nerve conduction over segments of different length. Because the CMAPs have very low amplitude due to abnormal temporal dispersion, the slow return to baseline was more critical for the digitalization process. Negative deflections (upward) of the slow afterwave are considered artefactual and/or introduced during the signal digitalization and removed from the signals before deconvolution.

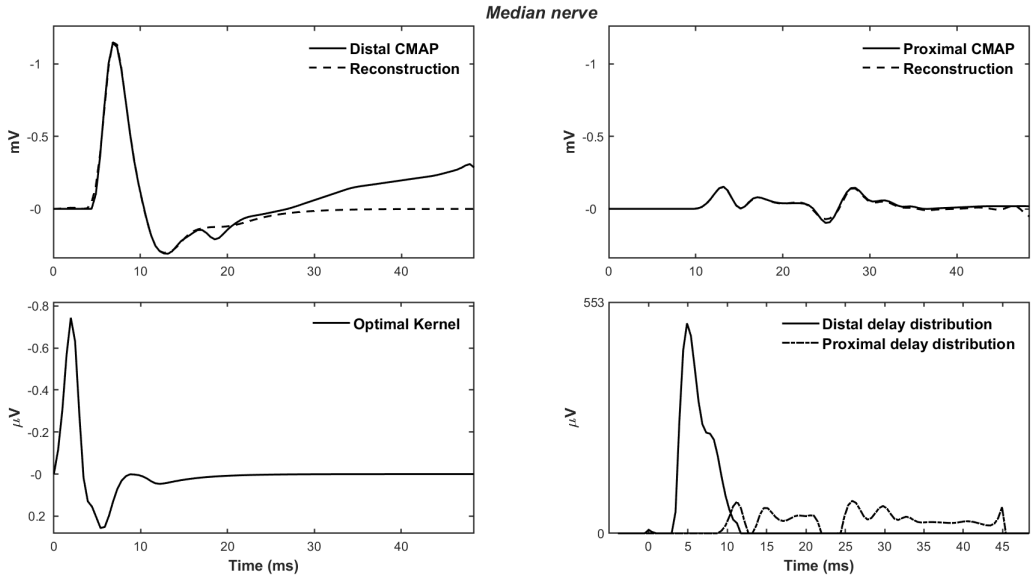

Figure 4.9: Example of deconvolution method operation on MNM signals. The CB is estimated from the signals elicited by median nerve stimulation, reported in Figure 4.8. The negative deviation (upward) of the distal CMAP is removed in the pre-processing step by sostitution of the fitted exponential, modelling the slow afterwave. Estimated CB = 35.8 %, Reconstruction error = 8.7 %.

	Conduction block (%)		
Studied nerve	**Amplitude**	**Area**	**Deconvolution**
Median			
wrist, elbow	86.6	79.1	35.8
Ulnar			
wrist, above elbow	79.8	32.4	8.1
below and above elbow	23.3	-5.3	6.6
Peroneal			
ankle, poplite	27.5	17.4	13.6
fibula, poplite	-34.3	-32.6	-10.5

Table 4.2: Conduction block estimation results for the MNM patient signals shown in Figure 4.8.

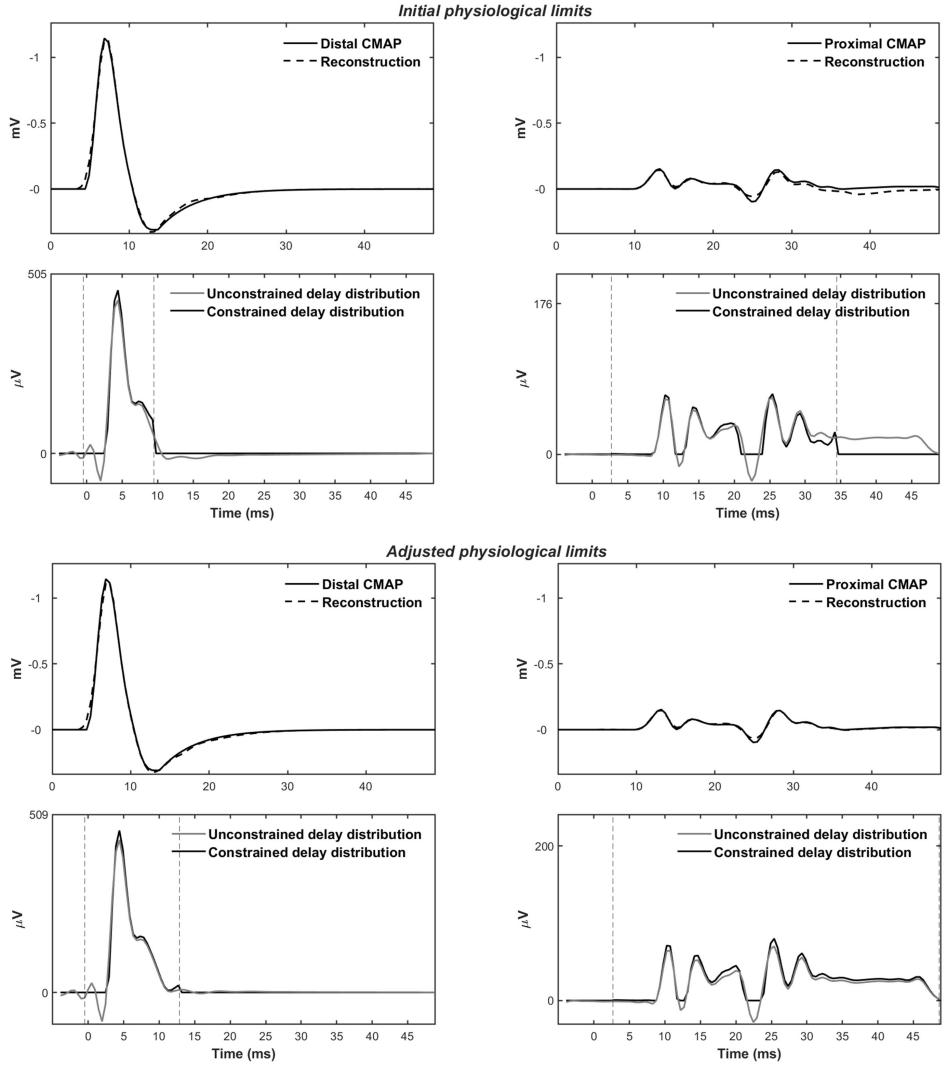

Figure 4.10: Example of physiological limits impact on the CB estimation with deconvolution. The CMAPs are recorded over the *Abp* muscle from a MNM patient. Evident abnormal temporal dispersion in the proximal CMAP. **Top**: Distances: 80 mm and 330 mm for the distal and proximal stimulation sites, respectively. Conduction velocities (CVN): 10 m/s and 80 m/s. Using these parameters the distal distribution is correctly constrained while the proximal is truncated around 35 ms. **Bottom**: The minimum CVN value is lowered to 7 m/s to better reconstruct the proximal CMAP. Note the important difference in the CB estimation related to the physiologic limits adjustment.

4.3 Statistical results

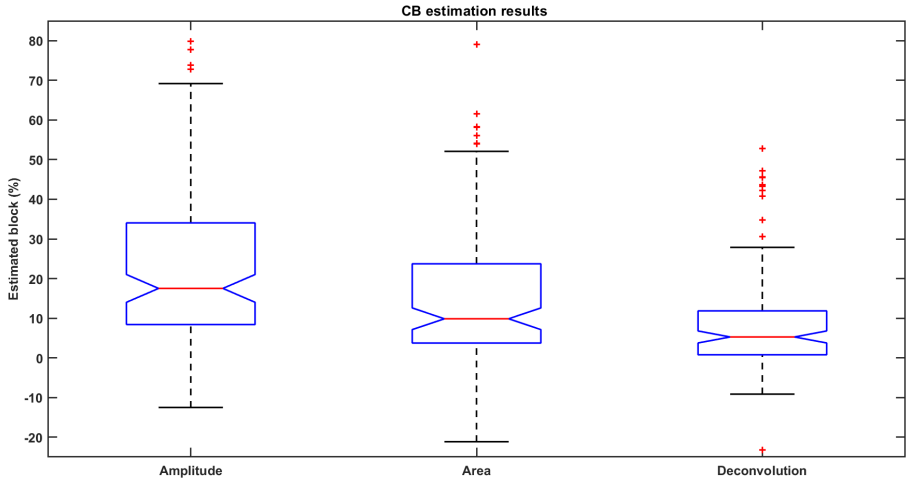

Figure 4.11: Analysis of variance of CB estimation with standard clinical methods and the deconvolution method on the full dataset.

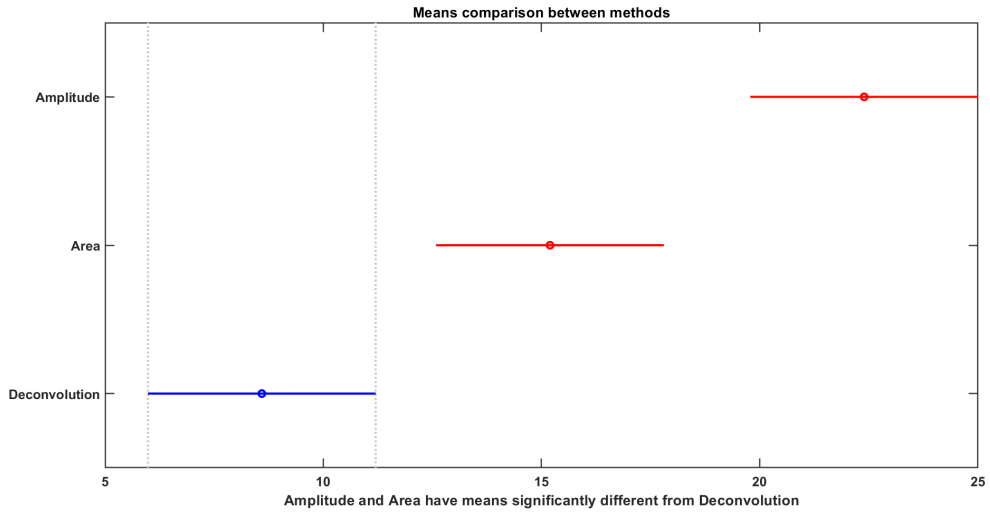

Figure 4.12: Multiple comparison test to identify significative difference between methods perfomances, considering the full dataset. Each group mean is represented by a symbol, and the comparison interval is represented by a line extending out from the symbol.

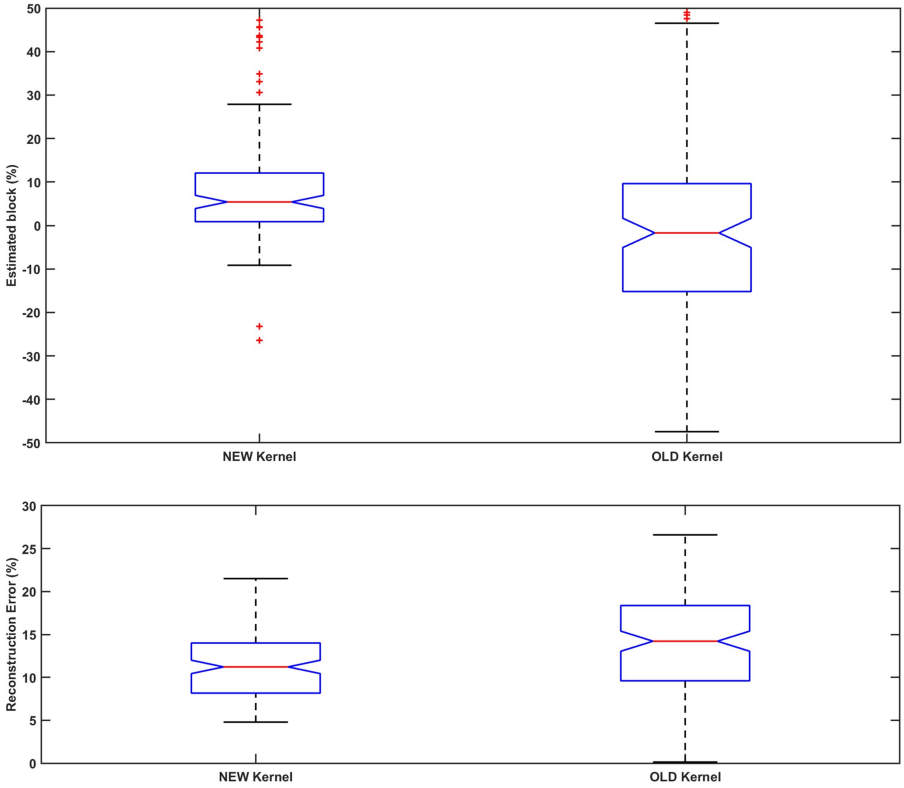

Figure 4.13: Comparison between the method performances using a kernel that model the slow return to baseline (NEW) or not (OLD). **Top**: Analysis of variance of the estimated CB on the full dataset. Using a kernel that models the slow afterwave, the variance of CB estimation is greatly reduced. **Bottom**: Decrease in reconstruction error when using the kernel that models the slow afterwave with respect to a kernel obtained exclusively with AH functions linear combination.

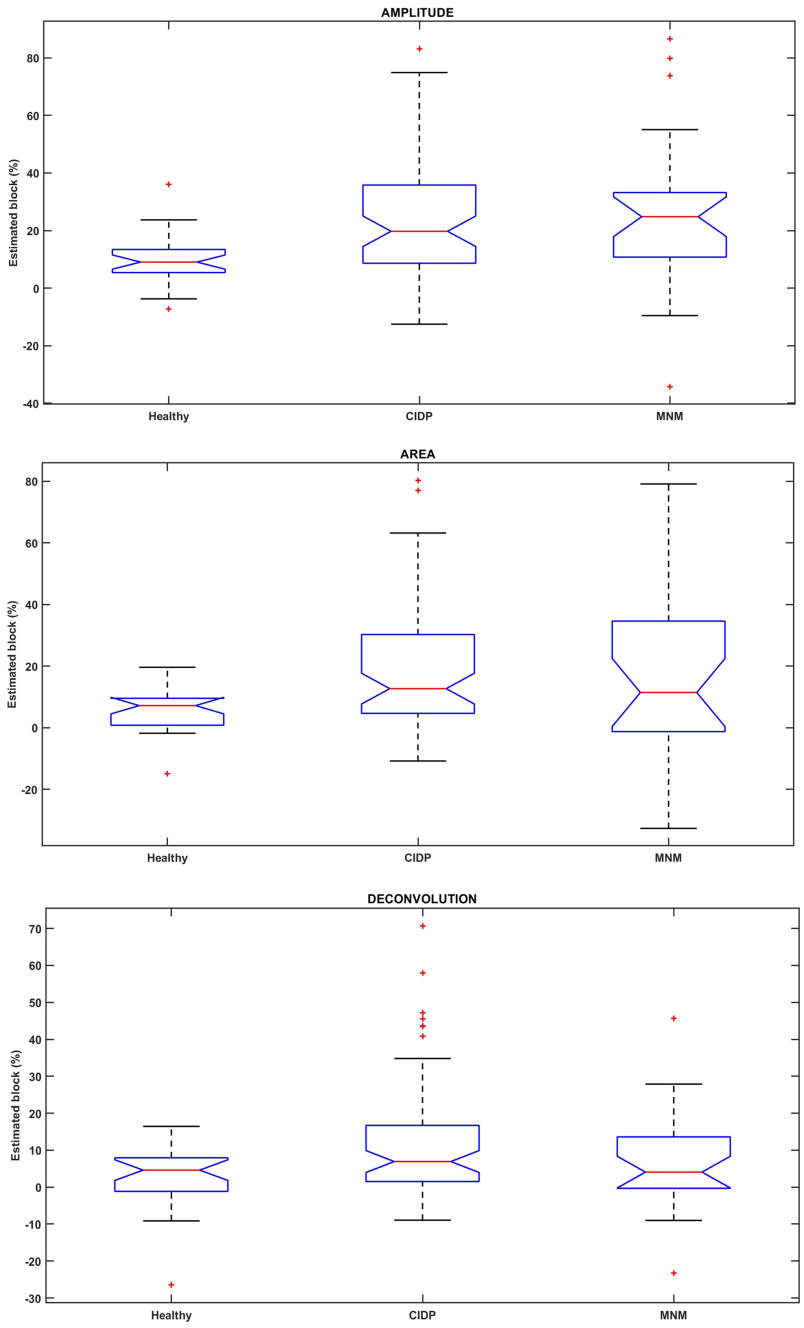

Figure 4.14: Analysis of variance of the estimated CB considering each method separately. Deconvolution allows to compensate phase cancellation effects that bias CB estimation in stardard clinical methods and to lower CB estimation variability especially in pathological subjects.

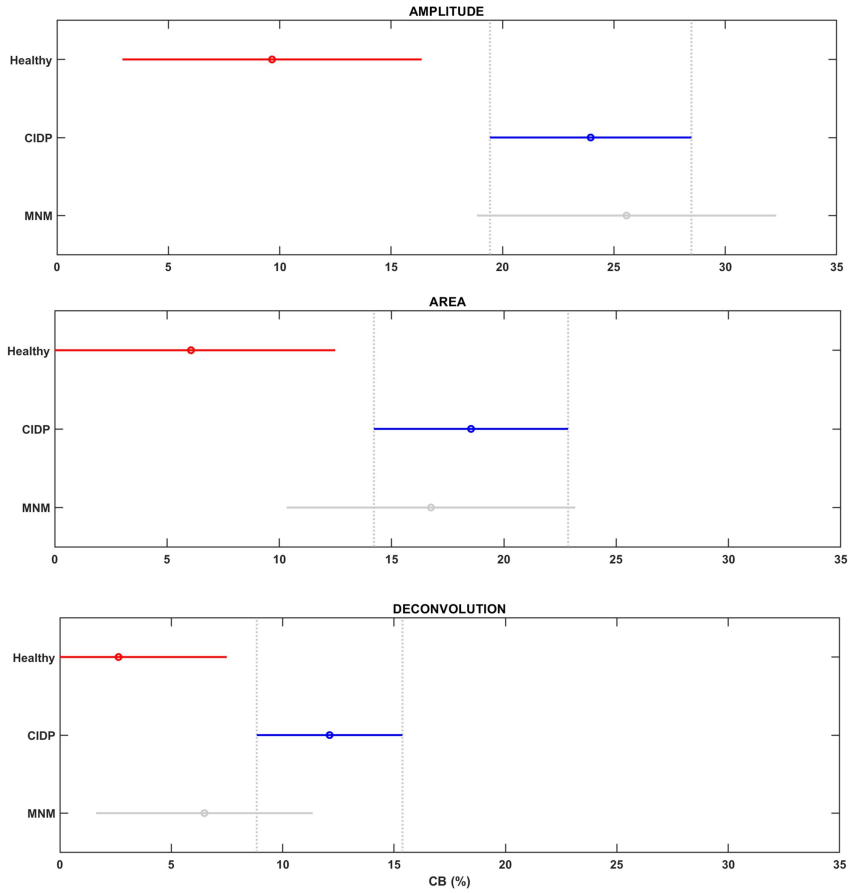

Figure 4.15: Multiple comparison tests to identify significative difference between subject groups for each method, considering the full dataset. For each method, the CB estimations from healthy and CIDP groups are significantly different ($p<0.05$). Deconvolution not only compensate the bias due to abnormal temporal dispersion affecting area and amplitude but allows to better differentiate CIDP from MNM patients on the basis of the estimated CB (comparison between blue and grey lines in each plot).

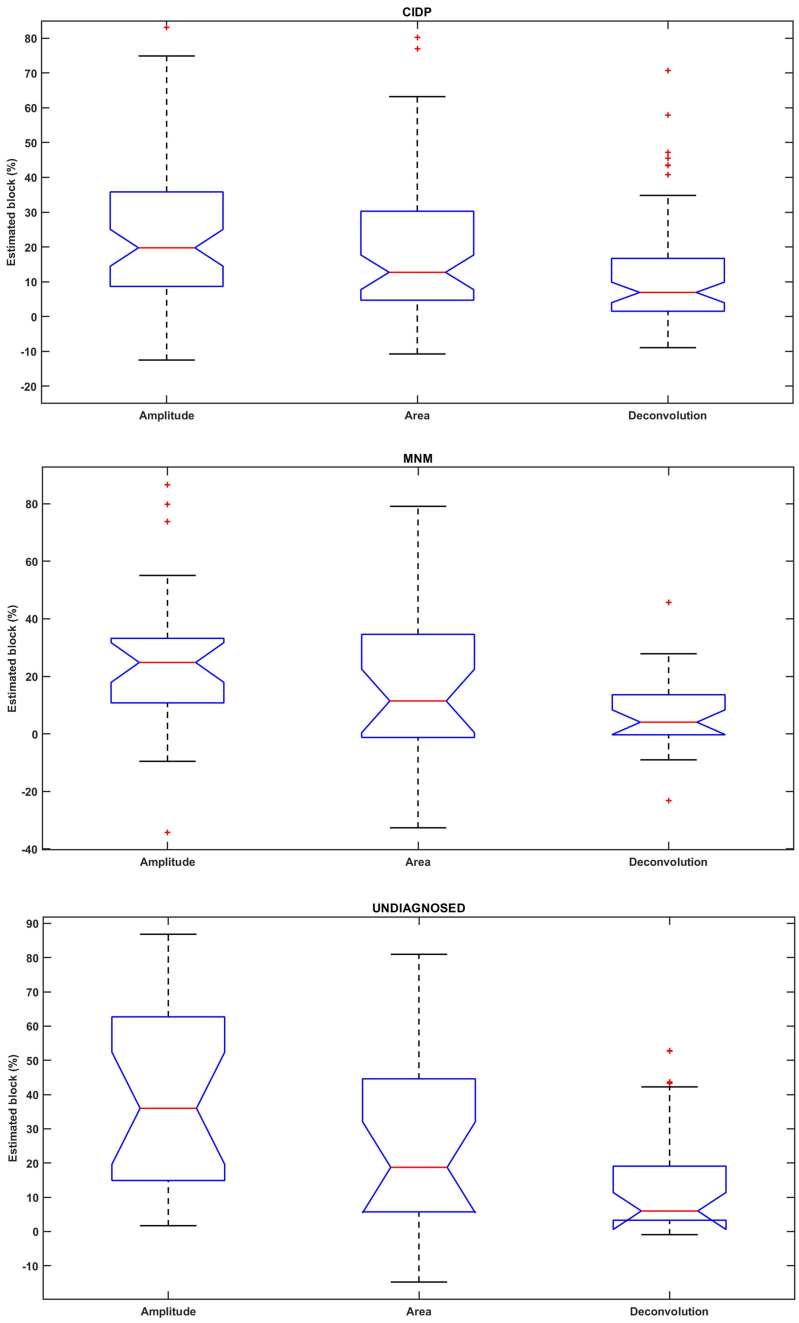

Figure 4.16: Analysis of variance of the estimated CB considering each group of pathological subjects separately. Deconvolution method results in less spread CB estimations for each group. The most significative difference refers to MNM patients, where area and amplitude methods fail to estimate CB correctly.

Chapter 5

Discussion and conclusions

In this thesis, we developed the novel method for CB estimation based on deconvolution of the CMAP introduced in [19] for its application to pathological subjects. The method was applied to experimental signals, focusing mostly on patients suffering from either CIDP or MNM. Both pathologies belong to the family of chronic autoimmune neuropathies.

5.1 Discussion of tests performed on healthy subjects

All the healthy signals were related to ulnar nerve stimulation. The CB was estimated with deconvolution, area and amplitude methods, comparing stimulation above-elbow with below-elbow and above-elbow with wrist. These two comparison are commonly performed during an ulnar nerve motor NCS, since it is usually very important to assess the nerve conduction in the forearm as well as across the elbow (see Figure 4.2 for an example). For the healthy subjects, the delay distributions were constrained considering $\mathrm{CVN}_{min} = 30$ m/s and $\mathrm{CVN}_{max} = 80$ m/s. Using this values, it was possible to effectively constrain each delay distribution to its physiological range. In addition, the distances between stimulation sites were measured. Knowing both the limits of CVN and the conduction distances, it was trivial to identify the time delay limits $\left[\frac{d}{CVN_{\max}}, \frac{d}{CVN_{\min x}}\right]$ used to constrain the delay distributions.
Further, these signals were originally digitalized. Hence no additional uncertainty (i.e. noise), related to the manual digitalization was added on the CMAPs by the user. The above described factors represent the best conditions to apply the deconvolution method, limiting at best the factors influencing the CB estimation related to user operations and choices.

The application on experimental signals is shown in Figure 4.3 and Figure 4.4.

The difference in the conduction distance determines different temporal dispersion in the signals. Note that the estimated delay distributions are very similar to ideal gaussian shapes, implying no demyalination in the studied nerve as the nerve APs arrive at the muscle within a short period of time. It should be noted that there is a great resamblance of shape between the recorded CMAPs and the optimal estimated kernel, further assessing the absence of abnormal temporal dispersion in the healthy nerve.

However, physiologic temporal dispersion is sufficient to positively bias methods based on area and amplitude, as indicated by the boxplots in Figure 4.4. These methods estimated a larger CB for increasing conduction distance, i.e., when comparing above-elbow with wrist with respect to the case of comparing above-elbow with below-elbow. Hence, our results confirm that the standard clinical methods are sensitive to temporal dispersion, as discussed in many papers ([31], [18]).
On the other hand, deconvolution method shows good stability with respect to temporal dispersion on this set of experimental healthy signals.

All the signals shown in Figure 4.1 return to the baseline with the slow afterwave. As discussed in Section3.2, this component arises from the the slow repolarization of the muscle fibers (represented by the IAP negative afterpotential). An example of the impact of modelling this component in the kernel to recostruct healthy signals is shown in Figure 4.2. In that case, an important decrease of the reconstruction error was obtained (from 18.5% to 9.9%) but almost no difference in the CB estimation was found (8.4% to 8.9%) when comparing the kernel without or with slow afterwave. The reason behind this is that the estimated delay distributions were very narrow in time, as described above, and there was great similarity between distal and proximal CMAPs. This similarity in shape determined poor effect of the slow afterwave in the kernel on the estimated CB, since the CMAPs returned to the baseline with almost identical exponential components.
Finally, it should be noted that the slow afterwave in surface recorded CMAPs could appear attenuated or distorted if the high pass filter cut-off frequency of the EMG machine is above 10 Hz. In this study, the slow afterwave was clearly visible on all the healthy signals, since the cut-off frequency was 2 Hz.

The proposed method performed better than either area or amplitude based methods when applied to experimental signals obtained from healthy subjects. Both area and amplitude based methods were biased by the temporal dispersion related to different conduction distance between stimulation sites, while the deconvolution was proven to be stable to temporal dispersion.

5.2 Discussion of tests performed on patients

The CB was estimated with deconvolution, area and amplitude methods on patients affected by Chronic Inflammatory Demyelinating Polyneuropathy (CIDP), Multifocal Motor Neuropathy (MMN) or undiagnosed neuropathies.
The above described demyelinating diseases are classified as rare so it was challenging to obtain a good number of experimental signals to test the deconvolution method for CB estimation. For this reason we decided to include in the pathological dataset the "undiagnosed" group, containing signals that were acquired from either CIDP or MNM patients but whose diagnosis was not provided by Dr.Cocito.

To perform CB estimation, two CMAPs are always required. For this reason, the method was tested on a dataset consisting of CMAP pairs. The full dasaset of signals used to test the method on patients was the following:

- 65 CMAP pairs from CIDP patients
- 26 CMAP pairs from MNM patients
- 21 CMAP pairs from undiagnosed patients

Each pair determines a comparison aiming to study the conduction along a nerve segment of length equal to the conduction distance between the stimulation sites used to evoke the motor responses.
Since the CMAPs were elicited by the stimulation of different nerves and the distance of the stimulation sites from the recorded muscle was rarely provided, it was not possible to divide the pathological dataset between high and low conduction distances as we did for the healthy subjects and the results analysis was based exclusively on the pathologies and the CB estimation methods.

We expected to find an higher difference between the performances of the deconvolution method and standard clinical methods performing tests on the pathological dataset with respect to what we found using the healthy subjects. This is due to the abnormal temporal dispersion affecting pathological signals, which sums to the physiologic dispersion related to the conduction distance, further increasing the phase cancellations effect on the recorded CMAPs.
This expectation was found to be true, as reported by the analysis of variance in Figure 4.14, in which the results for each method are displayed. The boxplots also clearly show that the deconvolution method allows to obtain less spread CB estimations for both CIDP and MNM groups with respect to area and amplitude based methods.
In addition, for both MNM and CIDP patients, the average estimated CB with deconvolution was lower than the average estimated CB with the other methods. This result shows the method's capability of compensating the phase cancellations

effect on the pathological signals. The analysis was performed with ANOVA, using an unbalanced design since our dataset was unbalanced between pathological groups. All the methods had significant impact on the results ($p < 0.05$). In particular, the proposed method had a significant impact on the estimated CB between healthy, CIDP and MNM subjects, $F = 4.22$, $p = 0.017$.
Starting from this significant results, post-hoc tests were performed for each method aiming to identify which method allowed better differentiation between the CIDP and MNM groups on the basis of the estimated CB. Every post-hoc test consisted in multiple comparisons between each group (healthy, CIDP, MNM) means to see if there was a significant difference between them. The results of this important tests are reported in Figure 4.15. For each method, the means of the healthy and CIDP groups were significantly different (red and blue lines, $p < 0.05$). The means of the CIDP and MNM groups were never significantly different with 5% significance level. However, the greater difference between CIDP and MNM groups means was obtained with the deconvolution method (blue and grey lines). This points towards the conclusion that the proposed method allows better distinction between CIDP and MNM patients on the basis of estimated CB with respect to area and amplitude based methods, which is an important result. MNM patients have the motor CB with a lower incidence that CIDP patients since their primary pathophysiologic consequence of demyelination is abnormal temporal dispersion. The abnormal temporal dispersion for these patients is particularly critical for the standard clinical methods used to estimate motor CB.
Deconvolution allows to compensate phase cancellation effects which are particularly important in MNM, detecting CB more reliably.

Now let's consider each pathological group separately. The analysis of variance results are reported in Figure 4.16. For each pathological group, ANOVA testing gave evidence of a difference between each method ($p < 0.05$) and, by performing the same multicompare tests as in Figure 4.15, it was confirmed that in all cases there was a significant difference between amplitude and deconvolution methods ($p < 0.05$). The means of area and deconvolution methods were not significantly different with 5% significance level in each group. The absence of significant difference was found also between amplitude and area methods for each group. Our opinion is that by increasing the population size and using a balanced dataset, statistically evidence of the difference between area and deconvolution methods could be found. However, for each considered pathological group, the CB estimations with the deconvolution method were less variable among subjects than the area and amplitude based methods. Notably, the greatest difference in CB estimation variance between standard methods and deconvolution was found with MNM patients in which the phase cancellation effects due to abnormal temporal dispersion were on average higher than CIDP patients.

This difference in the CMAPs between the two pathologies can be seen by comparing Figure 4.5 and Figure 4.8: it is evident that CIDP signals have a lower temporal dispersion than MNM. Referring to these two figures, the results of the CB estimation with amplitude, area, deconvolution methods are reported in Tables 4.1 and 4.2 for the CIDP and MNM signals, respectively. In both tables, considering the ulnar and peroneal nerve results, it is clear that amplitude and area methods CB estimation were positively biased by the larger conduction distances. This finding is in line with the results obtained by testing the method on healthy subjects. Note that the comparison between stimulation at the fibula and at the poplite in the MNM patient gave negative CB estimation with all the methods (Table 4.2). Because of this, we can be relatively sure that the stimulation at fibula (in this case) was not supramaximal.
Furthermore, the deconvolution method performance are reported for a CIDP example and a MNM example in Figure 4.6 and Figure 4.9, respectively. It is important to assess that in the CIDP example the CB presence is well estimated by both area and deconvolution methods since there is low temporal dispersion between the distal and proximal CMAPs. On the other hand, in the MNM example, the proximal CMAP is extremely dispersed in time causing an important CB overestimation with both amplitude (CB = 86.6%) and area (CB = 79.1%) methods. Deconvolution allows to compensate the phase cancellations by estimating the delay distributions, resulting in estimated CB = 35.8%.

Finally, we decided to compare the deconvolution method performances with area and amplitude methods using all the experimental signals at hand (both healthy and pathological), by using the "full dataset". One-way ANOVA indicated that the method used to estimate CB had a significant impact on the results ($p < 0.05$). From the boxplot in Figure 4.11 we can identify the deconvolution method as one of statistical relevance in CB estimation, giving less variable results on the full dataset with respect to area and amplitude based methods. The multicompare test results in Figure 4.12 further shows the significant difference between deconvolution and standard clinical methods when the full dataset is considered.

Figure 4.13 shows the impact of considering the slow afterwave in the kernel when testing the deconvolution method on the full dataset. The modelling of the slow return to the baseline in the kernel led to two important improvements in the deconvolution method:

- the standard deviations of the CB estimates performed on the full dataset decreased from 24.9% to 14%.
- the mean of the reconstruction error decreased from 15.7% to 11.7%.

The importance of considering the slow afterwave in the kernel is further displayed in details for a pathological subject in Figure 4.7. In this example, the

usage of a kernel which doesn't model the slow afterwave led to an erroneous CB estimation: $CB = -16.9\%$. This value emerges from the additional portion present in the proximal delay distribution pointed by the grey arrow. That additional portion interpretation is that, to reconstruct the proximal CMAP using the kernel without slow afterwave, additional delays are necessary. It is important to note that the addition portion of proximal distribution doesn't represent MUs activity but it is erroneously introduced to optimally reconstruct the signals. In particular, the convolution of the kernel with this portion of distribution results in the necessary phase cancellations to reproduce the slow return to baseline of the proximal CMAP. The optimal kernel which models the slow afterwave allowed to remove the erroneous portion of the proximal delay distribution (i.e., after around 13 ms) resulting in lower reconstruction error and $CB = 5.1\%$.

To conclude the results' discussion we have to describe two factors determining the deconvolution method application on experimental signals, focusing on the pathological subjects.

First of all, the majority of pathological signals was provided in the form of clinical records on paper and therefore needed to be manually digitalized to be processed in MATLAB (see Section 3.6 for details about the digitalization procedure). The manual idenfication of points over an image carries an intrinsic uncertainty related to the operator. This uncertainty led to addional noise on the signals, possibly introducing errors, especially when the signals had low amplitude (below 1 mV) and oscillates across the baseline.
In those cases, eventual negative drifts (upward) of the baseline were of difficult reproduction and their value was somewhat exaggerated with respect to the original signals (see Figure 4.8, distal CMAPs).

Another factor to consider is that the physiological limits have to be adjusted in each specific case. As discussed in Chapter 3, the estimated delay distributions are constrained to a time interval corresponding to physiological values of CVN, computed using the distances from each stimulation site. Note that the application of physiological limits to the delay distribution is a fundamental step to obtain reliable CB estimation via deconvolution. In the majority of cases, the distances at which the stimulation was performed during the NCS were not provided. In some other cases, the CVN was provided with the signals, hence it was possible to estimate the distances of the stimulation sites using both CMAPs onsets (PL and DL, proximal and distal, respectively) by using the following equation : $Distance = \mathrm{CVN}/(PL - DL)$. In any case, in general, the lack of precise measurements of the stimulation sites is an important disadvantage for CB estimation with the proposed method because it makes the time delay physiological limits definition more challenging. This is especially true for pathological signals related to patients who suffer from demyelinating diseases since the abnormal temporal dispersion results in CMAPs of longer duration than the healthy signals.

For each nerve (median, ulnar, peroneal), the distances of the stimulation sites were adjusted for each CMAP pair on which the CB was estimated, starting from the values reported in Table 5.1. The reported values were a good initial guess of the distances in the majority of CMAP pairs analyzed.
In pathological subjects, the minimum CVN could be 10 m/s or even less due to demyelination of some nerve fibers. Hence, it was not immediate to define the correct CVN interval since it was specific for each considered case. For the considered pathologies, we decided to perform CB estimation on patients considering CVN_{min} = 10 m/s and CVN_{max} = 80 m/s at first and to change these values for the specific case at hand (if necessary).
Considering all CIDP and MNM patients, the lower CVN_{min} used was 5 m/s and the higher CVN_{max} was 100 m/s.

	Distance (mm)	
Studied nerve	**Distal**	**Proximal**
Median		
wrist, elbow	80	330
Ulnar		
wrist, above elbow	80	430
below and above elbow	330	430
Peroneal		
ankle, poplite	110	550
fibula, poplite	450	550

Table 5.1: Reference values for the distance of distal and proximal stimulation sites in each studied nerve.

Figure 4.10 shows an example in which the physiological limits adjustment is crucial for the correct CB estimation. The reported signals are from a MNM patient, in which the proximal CMAP is extremely dispersed in time due to non-uniform conduction slowing. Using CVN_{min} = 10 m/s the proximal delay distribution is truncated and therefore the proximal CMAP is not well reconstructed. By lowering CVN_{min} to 7 m/s, the full distribution is considered and the CB estimation improves as displayed by the reconstruction error reduction.

5.3 Conclusions

In this work, the innovative method for CB estimation introduced by Prof. Luca mesin in [19] was developed for its application to experimental signals. Notably,

there was a great difference between healthy and pathological CMAPs recorded from patients suffering from demyelinating diseases. In this type of neuropathies, assuming normal conduction in the muscle, the main differences in CMAP size between an healthy and a pathological case are imputable to abnormal temporal dispersion.
The deconvolution method is based on important hypotheses that limit its applicability to CMAPs made up by biphasic MUAPs. For this reason, CMAPs recorded from subjects with axonal damage and possible collateral reinnervation, which are made up by polyphasic MUAPs, cannot be correctly elaborated via deconvolution. In particular, the phase cancellation due to polyphasia cannot be estimated by the method. It is therefore recommended to apply the deconvolution method for CB estimation only to signals that satisfy its hypotheses. We tested the deconvolution method on pathological signals related to demyelinating diseases since demyelination is the pathological basis of conduction block in human neuropathies. We focused on CIDP and MNM, both being acquired and chronic demyelinating diseases in which there is an immuno-mediated attack of the peripheral nerves.

Extensive study of the literature was necessary to understand the normal electrogenesis of a CMAP and how its shape could be affected by the clinical consequences of demyelinating neuropathies, namely abnormal temporal dispersion and conduction block. The slow return to baseline in surface potentials was analyzed in depth to understand its origin (which is physiological, [23]) and its impact on the deconvolution of the CMAPs.
Further studies are necessary to completely understand the slow afterwave presence on surface recorded EMG signals, possibly with the application of simulation models that use the IAP model as a starting point. In addition, an in-depth study of the terminal phase of the CMAP detected by belly-tendon electrodes could reveal the distinction between the effects of the IAP shape and its negative afterpotential from the higher desynchronization in muscle fiber activation. Nevertheless, we found a good solution to cope with the slow afterwave in experimental signals recorded from both healthy and pathological subjects by considering a kernel which contained the slow return to baseline.
The software computation time depends on the time support considered for the CMAPs and the corrispective samples. By using at maximum 100 ms and a sampling frequency of 2048 Hz as we did in this work, the computation time was of the order of 1 min with CPU 2.5 GHz and RAM 4GB.

Looking at future improvements, two main aspects of the method should be discussed. First, the application software contains several optimization procedures that could be further improved by using more sophisticated algorithms. Second, the adjustement of physiological limits on the specific case represents a drawback for the method applicability. Automatized adjustment procedures to identify the

physiological limits in each specific case would make the deconvolution method more robust to the high variability of patient-specific parameters (namely CVN limits and conduction distances).

Several critera for CB estimation have been published. These criteria usually require a decrease in amplitude or area for proximal CMAP relative to distal CMAP ranging from 20% to 60%, with the certainty of the block depending on the degree of temporal dispersion. For example, the American Academy of Neurology proposed a criterion for CB a more than 20% drop in area or peak-to-peak amplitude (distal vs proximal CMAP) with less than a 15% change in the duration.
The deconvolution method can overcome the detrimental effect of temporal dispersion on CB estimation from motor responses. In each pathological group we tested (CIDP, MNM, undiagnosed) it was found an evident positive biasing of the area and amplitude methods due to high temporal dispersion.
Based on the statistical results, we can conclude that the deconvolution method allowed to obtain less variable CB estimations among patients with a definite pathology than the standard clinical methods. The immediate consequence of this result is that better differentiation between CIDP and MNM patients can be obtained when estimating the motor CB with the proposed method with respect to area and amplitude methods.
Finally, our results indicate that the deconvolution method performed better in pathological subjects affected by abnormal temporal dispersion (TD), allowing to separate the contribution of CB and abnormal TD on the recorded CMAPs. On the other hand, area and amplitude based methods may fail to be diagnostically efficient in situations where both conduction block and abnormal temporal dispersion are present.

This work represents an important foundation for future clinical studies in which the deconvolution method could be applied to a wide range of pathological signals to define standardized criteria for the CB estimation in demyelinating neuropathies.

Bibliography

[1] Mark A Ferrante, B Teresa Spiegelberg, and BE Tsao. «Principles of Nerve Conduction Studies and Needle EMG». In: *American Association of Neuromuscular & Electrodiagnostic Medicine: Rochester, NY, USA* (2014) (cit. on pp. 1, 14).

[2] Arup Mallik and AI Weir. «Nerve conduction studies: essentials and pitfalls in practice». In: *Journal of Neurology, Neurosurgery & Psychiatry* 76.suppl 2 (2005), pp. ii23–ii31 (cit. on p. 2).

[3] Kerry H Levin. «Nerve Conduction Studies: Practical Physiology and Patterns of Abnormalities». In: *Acta Neural Belq* 106.2 (2004), pp. 73–81 (cit. on p. 2).

[4] John C Kincaid. «The compound muscle action potential and its shape». In: *Muscle and Nerve* 22.1 (1999), pp. 4–5 (cit. on p. 7).

[5] Kevin C MCGill and Zoia C Lateva. «The contribution of the interosseous muscles to the hypothenar compound muscle action potential». In: *Muscle & nerve* 22.1 (1999), pp. 6–15 (cit. on p. 7).

[6] Javier Rodriguez-Falces and Nicolas Place. «Determinants, analysis and interpretation of the muscle compound action potential (M wave) in humans: implications for the study of muscle fatigue». In: *European journal of applied physiology* 118.3 (2018), pp. 501–521 (cit. on p. 8).

[7] Zoia C Lateva, Kevin C McGill, and Charles G Burgar. «Anatomical and electrophysiological determinants of the human thenar compound muscle action potential». In: *Muscle & Nerve: Official Journal of the American Association of Electrodiagnostic Medicine* 19.11 (1996), pp. 1457–1468 (cit. on pp. 8, 29).

[8] John C Kincaid, Allison Brashear, and Omkar N Markand. «The influence of the reference electrode on CMAP configuration». In: *Muscle & Nerve: Official Journal of the American Association of Electrodiagnostic Medicine* 16.4 (1993), pp. 392–396 (cit. on p. 8).

[9] Javier Rodriguez-Falces, Armando Malanda, Iban Latasa, Ana Lavilla-Oiz, and Javier Navallas. «Influence of timing variability between motor unit potentials on M-wave characteristics». In: *Journal of Electromyography and Kinesiology* 30 (2016), pp. 249–262 (cit. on p. 9).

[10] J Gert van Dijk, WIM Van der Kamp, Bob J van Hilten, and Paul van Someren. «Influence of recording site on CMAP amplitude and on its variation over a length of nerve». In: *Muscle & Nerve: Official Journal of the American Association of Electrodiagnostic Medicine* 17.11 (1994), pp. 1286–1292 (cit. on p. 10).

[11] TE Feasby, WF Brown, JJ Gilbert, and AF Hahn. «The pathological basis of conduction block in human neuropathies.» In: *Journal of Neurology, Neurosurgery & Psychiatry* 48.3 (1985), pp. 239–244 (cit. on p. 14).

[12] Jun Kimura. «Facts, fallacies, and fancies of nerve conduction studies: Twenty-first annual Edward H. Lambert lecture». In: *Muscle & Nerve: Official Journal of the American Association of Electrodiagnostic Medicine* 20.7 (1997), pp. 777–787 (cit. on p. 17).

[13] Mazen M Dimachkie and Richard J Barohn. «Chronic inflammatory demyelinating polyneuropathy». In: *Current treatment options in neurology* 15.3 (2013), pp. 350–366 (cit. on p. 17).

[14] Richard K Olney and Robert G Miller. «Conduction block in compression neuropathy: recognition and quantification». In: *Muscle & Nerve: Official Journal of the American Association of Electrodiagnostic Medicine* 7.8 (1984), pp. 662–667 (cit. on p. 22).

[15] Wilhelm J Schulte-Mattler, Tobias Müller, Dimitrios Georgiadis, Malte E Kornhuber, and Stephan Zierz. «Length dependence of variables associated with temporal dispersion in human motor nerves». In: *Muscle & Nerve: Official Journal of the American Association of Electrodiagnostic Medicine* 24.4 (2001), pp. 527–533 (cit. on p. 23).

[16] Erik Stålberg and Lars Karlsson. «The motor nerve simulator». In: *Clinical neurophysiology* 112.11 (2001), pp. 2118–2132 (cit. on p. 23).

[17] Sergiy Reutskiy, Enrico Rossoni, and Brunello Tirozzi. «Conduction in bundles of demyelinated nerve fibers: computer simulation». In: *Biological cybernetics* 89.6 (2003), pp. 439–448 (cit. on p. 23).

[18] Edward K Rhee, John D England, and Austin J Sumner. «A computer simulation of conduction block: effects produced by actual block versus interphase cancellation». In: *Annals of Neurology: Official Journal of the American Neurological Association and the Child Neurology Society* 28.2 (1990), pp. 146–156 (cit. on pp. 24, 68).

[19] Luca Mesin and Dario Cocito. «A new method for the estimation of motor nerve conduction block». In: *Clinical neurophysiology* 118.4 (2007), pp. 730–740 (cit. on pp. 25, 41, 48, 67, 73).

[20] Pariwat Thaisetthawatkul, Eric L Logigian, and David N Herrmann. «Dispersion of the distal compound muscle action potential as a diagnostic criterion for chronic inflammatory demyelinating polyneuropathy». In: *Neurology* 59.10 (2002), pp. 1526–1532 (cit. on p. 27).

[21] Sagiri Isose et al. «Utility of the distal compound muscle action potential duration for diagnosis of demyelinating neuropathies». In: *Journal of the Peripheral Nervous System* 14.3 (2009), pp. 151–158 (cit. on p. 27).

[22] Zoia C Lateva and Kevin C McGill. «Estimating motor-unit architectural properties by analyzing motor-unit action potential morphology». In: *Clinical neurophysiology* 112.1 (2001), pp. 127–135 (cit. on p. 29).

[23] Zoia C Lateva and Kevin C McGill. «The physiological origin of the slow afterwave in muscle action potentials». In: *Electroencephalography and Clinical Neurophysiology/Electromyography and Motor Control* 109.5 (1998), pp. 462–469 (cit. on pp. 31, 32, 74).

[24] HP Ludin. «Microelectrode study of normal human skeletal muscle». In: *European neurology* 2.6 (1969), pp. 340–347 (cit. on p. 32).

[25] Kevin C McGill, Zoia C Lateva, and Shaojun Xiao. «A model of the muscle action potential for describing the leading edge, terminal wave, and slow afterwave». In: *IEEE transactions on biomedical engineering* 48.12 (2001), pp. 1357–1365 (cit. on pp. 32, 41).

[26] GV Dimitrov. «Influence of the afterpotentials on the shape and magnitude of the extracellular potentials generated under activation of excitable fibres». In: (1979) (cit. on p. 32).

[27] GV Dimitrov, ZC Lateva, and NA Dimitrova. «Model of the slow components of skeletal muscle potentials». In: *Medical and Biological Engineering and Computing* 32.4 (1994), pp. 432–436 (cit. on p. 32).

[28] Todor I Arabadzhiev, George V Dimitrov, Vichren E Chakarov, Alexander G Dimitrov, and Nonna A Dimitrova. «Effects of changes in intracellular action potential on potentials recorded by single-fiber, macro, and belly–tendon electrodes». In: *Muscle & Nerve: Official Journal of the American Association of Electrodiagnostic Medicine* 37.6 (2008), pp. 700–712 (cit. on p. 34).

[29] Andrey N Tikhonov and Vasiliy Y Arsenin. «Solutions of ill-posed problems». In: *New York* 1 (1977), p. 30 (cit. on p. 37).

[30] LR Lo Conte, Roberto Merletti, and Guido V Sandri. «Hermite expansions of compact support waveforms: applications to myoelectric signals». In: *IEEE Transactions on Biomedical Engineering* 41.12 (1994), pp. 1147–1159 (cit. on p. 40).

[31] Richard K Olney, Hans J Budingen, and Robert G Miller. «The effect of temporal dispersion on compound action potential area in human peripheral nerve». In: *Muscle & Nerve: Official Journal of the American Association of Electrodiagnostic Medicine* 10.8 (1987), pp. 728–733 (cit. on pp. 48, 68).